NASA TECHNICAL NOTE
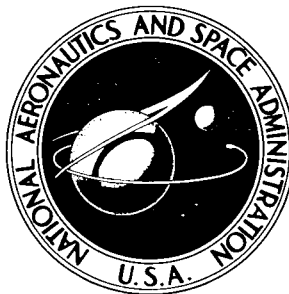
NASA TN D-1962

SUPERSONIC INVESTIGATION OF NOZZLE HINGE MOMENTS OF A MODIFIED SATURN C-1 MODEL WITH AND WITHOUT JET FLOW

by Nickolai Charczenko and Jerry L. Lowery

Langley Research Center

Langley Station, Hampton, Va.

TECHNICAL NOTE D-1962

SUPERSONIC INVESTIGATION OF NOZZLE HINGE MOMENTS

OF A MODIFIED SATURN C-1 MODEL

WITH AND WITHOUT JET FLOW

By Nickolai Charczenko and Jerry L. Lowery

Langley Research Center
Langley Station, Hampton, Va.

NATIONAL AERONAUTICS AND SPACE ADMINISTRATION

NATIONAL AERONAUTICS AND SPACE ADMINISTRATION

TECHNICAL NOTE D-1962

SUPERSONIC INVESTIGATION OF NOZZLE HINGE MOMENTS

OF A MODIFIED SATURN C-1 MODEL

WITH AND WITHOUT JET FLOW

By Nickolai Charczenko and Jerry L. Lowery

SUMMARY

An investigation has been conducted in the Langley Unitary Plan wind tunnel
to determine the nozzle hinge-moment coefficients for the Saturn C-1 vehicle with
various shrouds at Mach numbers from 1.60 to 2.87. The model used in this inves-
tigation represented the first stage and a modified second stage of the Saturn C-1
configuration. Nozzle hinge-moment coefficients were obtained from pressure meas-
urements on one nozzle with and without simulated jet flow. In addition, pressure
measurements were obtained on one shroud and at the base of the model.

A limited analysis of the results of this investigation indicates that the
long shrouds result in small nozzle hinge-moment coefficients which are relatively
independent of gimbal angle, Mach number, and jet flow. When the shrouds are
shortened enough to allow significant impingement of the airstream on the nozzles,
nozzle gimbal angle, Mach number, and jet flow become important factors in deter-
mining the magnitude of nozzle hinge-moment coefficients.

INTRODUCTION

Among the many problems involved with the launch system for a space vehicle
is control of the system until first stage "dropoff." Control of such systems may
be either by aerodynamic means such as fins or by thrust-vector control achieved
by gimbaling the nozzles. The determining factors in selecting the type of con-
trol is usually based on a compromise of weight and the positive nature of the
control. With thrust-vector control, the aerodynamic forces acting on the nozzle
must be overcome in order to gimbal the nozzles to their required positions. One
means of reducing or eliminating the aerodynamic loads on the nozzles is by
shielding them with shrouds. However, complete shielding adds weight and pre-
sents structural difficulties; therefore, a compromise is necessary in order to
minimize the weight and structural problems and still maintain sufficiently low
aerodynamic moments for the gimbal actuators to overcome.

Inasmuch as the thrust-vector type of control has been selected for the Saturn C-1 launch vehicle, an investigation was initiated to determine the type and length of shrouds required for the vehicle. The tests were performed in the Langley Unitary Plan wind tunnel at Mach numbers from 1.60 to 2.87 (this Mach number range encompasses the anticipated maximum hinge-moments region), at angles of attack from $0°$ to $-8°$, and with nozzle gimbal angles from $3°$ inward to $12°$ outward, radially. Two types of shrouds were investigated, a single- and a double-flare shroud; the single-flare shroud was tested with three different lengths. The data were obtained by means of pressure orifices over the external nozzle surfaces both with and without flow through the nozzles. Pressure coefficients were also obtained over the surfaces of the shrouds and the base of the vehicle.

SYMBOLS

A area, sq ft

A_e nozzle exit area, sq ft

C_p pressure coefficient, $\dfrac{p_l - p_\infty}{q_\infty}$

ΔC_p incremental pressure coefficient due to strut interference, $C_{p,\text{strut on}} - C_{p,\text{strut off}}$

C_H nozzle hinge-moment coefficient

F_i section normal force, lb

i,k summation integers

l distance from nozzle pivot to exit plane, in.

l_i section moment arm, in.

M Mach number

M_H nozzle hinge moment, in-lb

M_i section moment, in-lb

p static pressure, lb/sq ft

p_j/p_∞ jet-to-free-stream static-pressure ratio

q dynamic pressure, lb/sq ft

r radial distance from model center line, in.

R	Reynolds number per foot

R   Reynolds number per foot

X,Y,Z   axis system (see Appendix)

x   distance forward of nozzle exit or end of shroud, in.

y   radial distance from nozzle center line, in.

α angle of attack, deg

ϕ meridian angle, deg

δ_n nozzle gimbal angle (measured radially with respect to the model center line), deg

Subscripts:

U   upper

L   lower

l local

j   jet exit

∞ free stream

WIND TUNNEL

The tests were conducted in the Langley Unitary Plan wind tunnel which is a variable-pressure return-flow tunnel. The test section is 4 by 4 feet in cross section and approximately 7 feet long. The Mach number may be continuously varied from 1.5 to 2.9 by means of an asymmetric sliding block without shutting down the tunnel. Further details of the tunnel may be obtained from reference 1.

MODEL AND SUPPORT SYSTEM

A schematic drawing of the model and support system is presented in figures 1 and 2(a). The model was of steel construction and represents the first two stages of the Saturn C-1 vehicle. The first stage is a 1.57-percent model and the second stage is modified by shortening the length and replacing the second-to-third-stage interface with a conical nose section. (A foreshortened version of the vehicle was necessary in order to test the model without tunnel shock-wave interference at M = 1.60 and to retain components large enough for the hinge-moment tests.) The model had a total of eight nozzles, four of which were clustered about the center of the base and the other four positioned 90° apart around the base periphery (see model base in fig. 2(b)). The inner four nozzles were fixed and alined parallel to the center line of the model. The outer four nozzles were canted 6°

radially outward in their normal position, but could be gimbaled radially from 3° inward to 12° outward. The nozzles were all designed to have an exit Mach number of 2.66; details and coordinates of the nozzles are presented in figure 3. Nozzles 2, 3, and 6 (see fig. 4) were instrumented with orifices for measuring external surface pressure distribution on the nozzles, and these orifices were located as shown in figure 5. In addition, nozzles 4 and 8 had orifices on the inner surface near the exit. (Data from these nozzles were used to compute jet-pressure ratios.) Thin plates representing heat shields were provided at the base of the model, one between the inner four nozzles (referred to in the tables as a "star") 1.454 inches from the base and the other 0.715 inch from the base. Heat shields were instrumented with pressure orifices as shown in figure 4. The heat shields closer to the base were removed for the tests with the shortest shroud.

The two basic shroud designs, single and double flare, used in this investigation are shown in figure 6. The two modified shrouds differed only in length from the single-flare design. The orifice locations on the shrouds are shown in figure 7. One shroud was instrumented for each configuration and this shroud was the one that shielded the number 2 nozzle. In addition to the regularly instrumented shrouds shown in figure 7, a single-flare basic shroud was instrumented with 37 pressure orifices, as shown in figure 8, to obtain a more detailed pressure distribution. For jet simulation tests, a high-pressure air supply was introduced to the model through holes in the swept strut-support system (see fig. 2(a)).

The air supply system available for jet simulation was capable of providing high-pressure air at a sustained flow rate of 2 pounds per second, or a maximum flow rate of about 11 pounds per second for about 10 seconds.

TESTS, MEASUREMENTS, AND DATA PRESENTATION

The tests were performed through a Mach number range from 1.60 to 2.87, at angles of attack from 0° to -8°, and with nozzle gimbal angles of 3° inward and 6° and 12° outward, radially. Static pressure measurements were obtained on the shrouds, the nozzles, the model bases, and at the nozzle exit. These pressures were obtained by means of pressure transducers which for the majority of the data were accurate to about ± 5 lb/sq ft. The accuracy of the hinge-moment coefficients is estimated to be ± 0.02 for the lowest value of q_∞.

Since it was necessary to test the model with a strut-support system, it seemed desirable to determine the interference effects of the strut on the various pressure measurements taken at and near the base of the model. Accordingly, a similar, wooden model was fabricated that could be sting supported with and without a strut attached. A drawing of this model and photographs are presented in figures 9 and 10, respectively. Pressure measurements were taken at locations shown in figure 11 for this model with and without the strut. The incremental pressure coefficient due to the strut is shown in figures 12 to 14, and, in general, this effect is small enough not to compromise the accuracy of the pressure measurements obtained for the test vehicle.

The nozzle hinge-moment coefficients presented herein were obtained from mathematical integration of the pressures measured on the number 2 nozzle. An outline of this type of integration is presented in the appendix to this paper. It should be kept in mind that the accuracy of the hinge-moment coefficients obtained in this manner is limited by the small number of pressure stations available.

Shown in table I are the test conditions for each configuration. Only a limited analysis has been made of the effect of various parameters on the nozzle hinge-moment coefficients derived from the pressure distribution on the number 2 nozzle, and these results are presented in figures 15 to 18.

Complete tabulations of the pressure data for all configurations have been calculated in coefficient form and are presented separately in a "Supplement to NASA TN D-1962" that may be obtained upon request to the NASA. A request form is included at the back of this paper.

RESULTS AND DISCUSSION

The effect of shroud geometry on the variation of nozzle hinge-moment coefficient with Mach number in the jet-off condition is presented in figure 15. The data in figure 15 indicate that shroud length and nozzle attitude are the important considerations concerning the magnitude of hinge-moment coefficients for nozzles on launch structures such as the Saturn C-1. When the nozzle is almost completely shielded from the airstream by a shroud such as is the case with either the single- or double-flare basic shroud, the nozzle hinge-moment coefficients are essentially zero at nozzle gimbal angles from 3° inward to 12° outward, and throughout the Mach number range from 1.60 to 2.87. With the shortest shroud length (shroud cut to firewall), there is a significant increase in nozzle hinge-moment coefficient at all test Mach numbers and a further increase in magnitude as the nozzle is gimbaled outward radially. For this shortest shroud condition, the data also indicate that, as increased portions of the nozzle are affected by airstream impingement due to gimbaling the nozzles outward, there is a decrease in hinge-moment coefficient with increasing Mach number. The hinge-moment coefficients for the intermediate-length shroud configuration (shroud cut to heat shield) are about zero for a gimbal angle of -3° at all test Mach numbers; however, with gimbal angles outward 6° and 12°, there is an appreciable increase in hinge-moment coefficient, although not nearly as great as for the configuration with the shroud cut to firewall. The effect of nozzle gimbal angle on the shorter shroud configurations may be seen more clearly in figure 16 which presents the effect of angle of attack on the variation of nozzle hinge-moment coefficient with gimbal angle in the jet-off condition. (See specifically figs. 16(c) and 16(d).) Figure 16 also shows there are only small effects of angle of attack to -8° on the variation of nozzle hinge-moment coefficient with nozzle gimbal angle for single- and double-flare basic shroud configurations. For the shorter shroud configurations, the effects due to angle of attack in some cases are comparable in magnitude to the jet-flow effects for these configurations.

The effect of jet pressure ratio on the variation of nozzle hinge-moment coefficient with gimbal angle at $\alpha = 0^\circ$ is presented in figure 17. This figure

indicates that there is little or no effect of jet flow on the basic shroud length configurations at any of the test Mach numbers. With the shroud cut to heat shield, some effects of jet pressure ratio on nozzle hinge-moment coefficients may be noted; however, these effects are generally of small magnitude compared with the effects obtained for the shortest shroud configuration. With the shroud cut to firewall there is an appreciable effect of jet flow. At $M = 1.60$, $\alpha = 0^\circ$, and $p_j/p_\infty = 3.4$, there is an almost constant increase in hinge-moment coefficient at all test gimbal angles as compared with the no-jet-flow condition. At the higher Mach numbers of the test and with higher ratios of p_j/p_∞, jet flow causes a decrease in hinge-moment coefficient. To inspect further this reversal of effect of jet flow on nozzle hinge-moment coefficients, the data for the shroud cut to firewall were plotted as a function of angle of attack at $M = 1.60$ and $M = 2.00$ for conditions with and without jet flow in figure 18. These data show the same reversal of effect of jet flow at $\alpha = 0^\circ$ noted in figure 17; however, at an angle of attack of -8°, the effect of jet flow is the same for both Mach numbers. Insufficient data were obtained to determine whether the reversal of jet flow effect at $\alpha = 0^\circ$ between $M_\infty = 1.60$ and $M_\infty = 2.00$ is caused by jet flow ratio or Mach number.

Shown in figures 19 to 22 are some typical schlieren photographs of the four shroud configurations at various test conditions.

CONCLUDING REMARKS

Tests of a modified Saturn C-1 model configuration to determine the nozzle hinge-moment coefficients with various shrouds at Mach numbers from 1.60 to 2.87 indicate the following:

1. Shroud length is the major factor influencing nozzle hinge moments on this type of vehicle.

2. When there is significant impingement of the airstream on the nozzle, the nozzle gimbal angle, Mach number, and jet flow become important factors in determining the magnitude of nozzle hinge-moment coefficients.

Langley Research Center,
National Aeronautics and Space Administration,
Langley Station, Hampton, Va., June 21, 1963.

APPENDIX

MATHEMATICAL INTEGRATION OF PRESSURES ON A NOZZLE
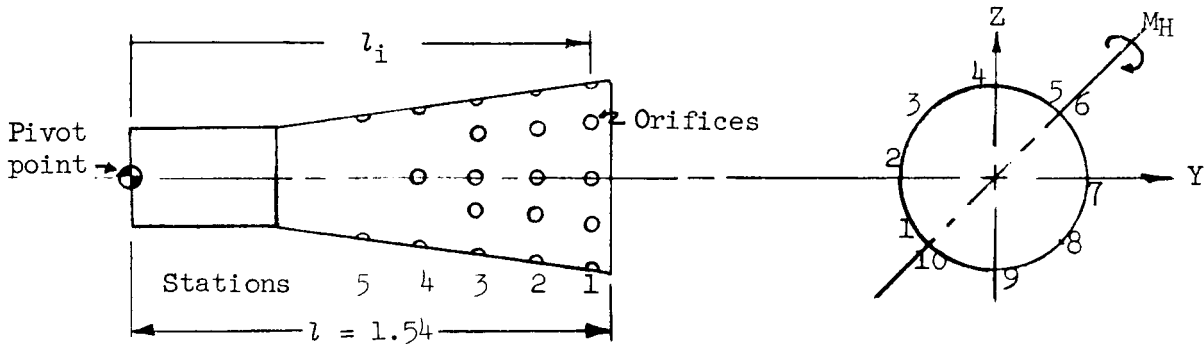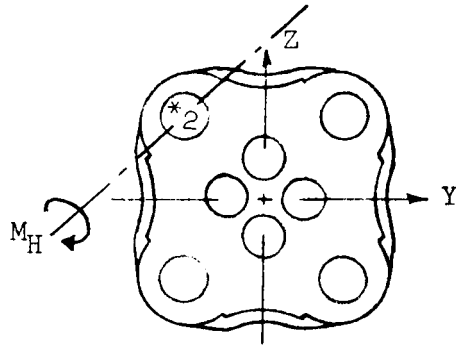
The nozzle hinge moment is determined from the pressure distribution on a nozzle based on the following assumptions:

1. Only normal component of pressure acting perpendicular to the X-axis of the nozzle contributes to the hinge moment.

2. At a given station, as indicated in the sketch, each measured pressure acts on an equal area.

Then the section normal force is:

$$F_i = \int_0^A \left(p_U - p_L \right) dA$$

or

$$F_i = \sum_{k=1}^5 p_k A_k - \sum_{k=6}^{10} p_k A_k$$

7

where p_k is the pressure at a particular orifice and A_k is the projected area associated with that orifice.

At a given station $A_2 = A_9$, $A_3 = A_8$, and $A_4 = A_7$

$$F_i = (p_2 - p_9)A_2 + (p_3 - p_8)A_3 + (p_4 - p_7)A_4$$

Then the section moment can be computed for that station as follows:

$$M_i = l_i F_i$$

where l_i is a section moment arm. Then the total nozzle hinge moment is:

$$M_H = \sum_{i=1}^{5} l_i F_i$$

from which the total nozzle hinge-moment coefficients are obtained:

$$C_H = \frac{M_H}{q_\infty A_e l}$$

8

REFERENCE

1. Anon.: Manual for Users of the Unitary Plan Wind Tunnel Facilities of the National Advisory Committee for Aeronautics. NACA, 1956.

TABLE I.- TEST CONDITIONS FOR EACH CONFIGURATION INVESTIGATED

x indicates specific test conditions investigated for configuration:*

M_∞	α, deg	R, per ft	q_∞, lb/sq ft	p_j/p_∞	A-1	A-2	A-3	A-4	B-1	B-2	B-3	B-4	C-1	C-2	C-3	C-4	D-1	E-1	F-5
1.60	Range**	2.9×10^{-6}	645	0	x	x	x	x	x	x	x	x	x	x	x	x	x		x
				2.8	x	x	x	x	x	x	x	x	x	x	x	x	x		x
				3.0	x				x	x	x	x	x	x	x	x	x		x
				3.4	x														
				3.9	x														
				4.5	x														
				4.8	x														
				6.5	x														
2.00	Range	2.5×10^{-6}	553	0	x	x	x	x	x	x	x	x	x	x	x	x	x		x
				5.1	x	x													
				5.5	x															
				6.3	x															
				7.1	x															
				8.3	x															
				8.7	x															
				11.9	x															
2.40	Range	2.0×10^{-6}	435	0	x	x	x	x	x	x	x	x	x	x	x	x			x
				9.4	x	x													
				10.1	x															
				11.4	x															
				12.8	x															
				15.4	x															
				16.0	x															
				21.4	x															
		2.4	540	9.3	x														
		2.4	540	12.8	x														
		1.5	327	15.3	x														
		1.5	327	21.4	x														
2.87	Range	1.6×10^{-6}	3.04	0	x	x	x	x	x	x	x	x	x	x	x	x		x	x
				18.9	x	x													
				20.5	x															
				25.6	x															
				25.3	x															
				31.2	x															
				42.2	x															

*CONFIGURATION CODE

[Letters A, B, C, . . . refer to nozzle conditions; numbers 1, 2, 3, . . . refer to shroud design]

	Nozzle
A	Nozzles 1, 2, 3, and 4 gimbaled 6° outward.
B	Nozzles 2 and 3 gimbaled 12° outward; nozzles 1 and 4 gimbaled 6° outward.
C	Nozzles 2 and 3 gimbaled 3° inward; nozzles 1 and 4 gimbaled 6° outward.
D	Nozzle 1 plugged; nozzles 2, 3, and 4 gimbaled 3° inward.
E	Nozzle 7 plugged; nozzles 1, 2, 3, and gimbaled 12° outward.
F	Nozzle 1 plugged; nozzles 2, 3, and 4 gimbaled 6° outward.

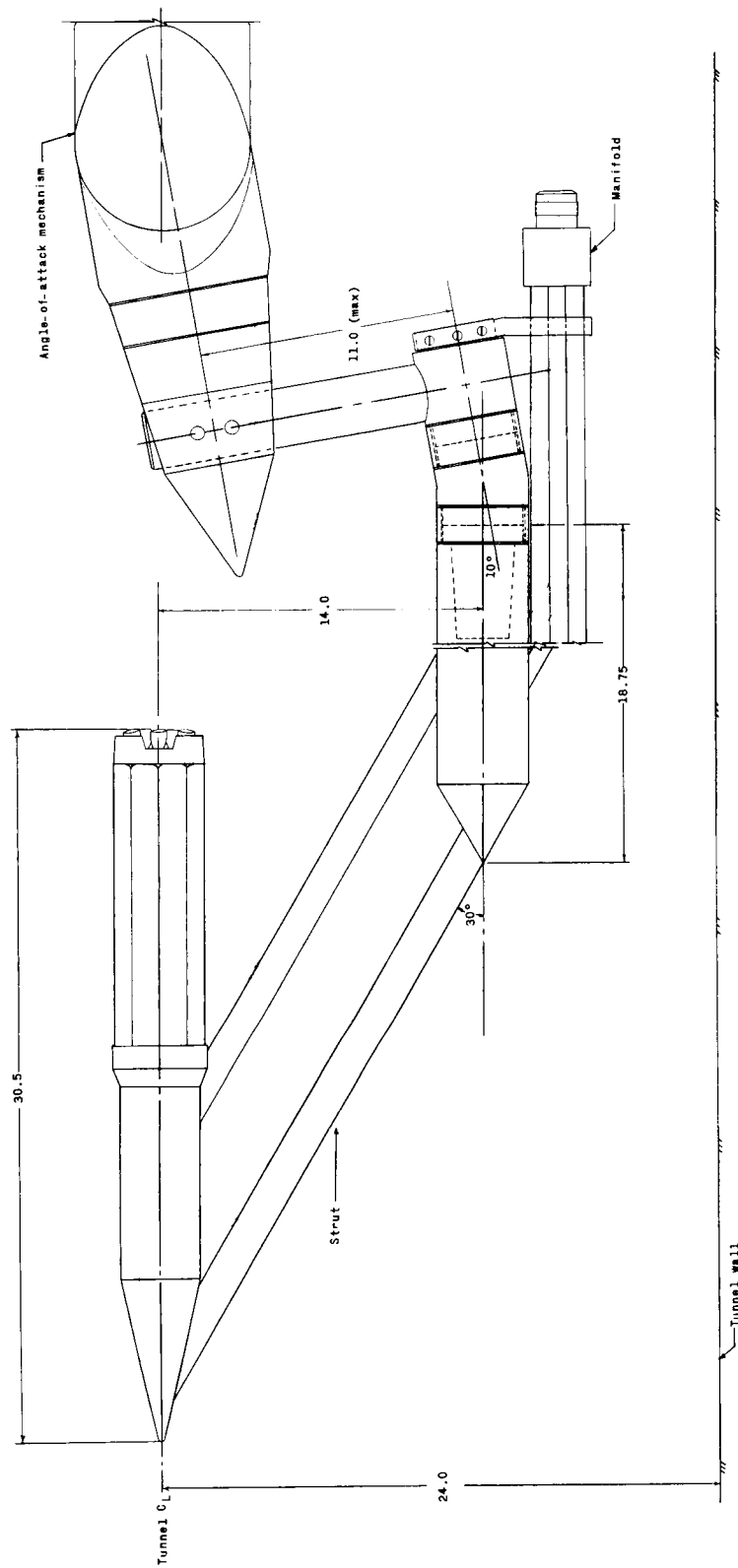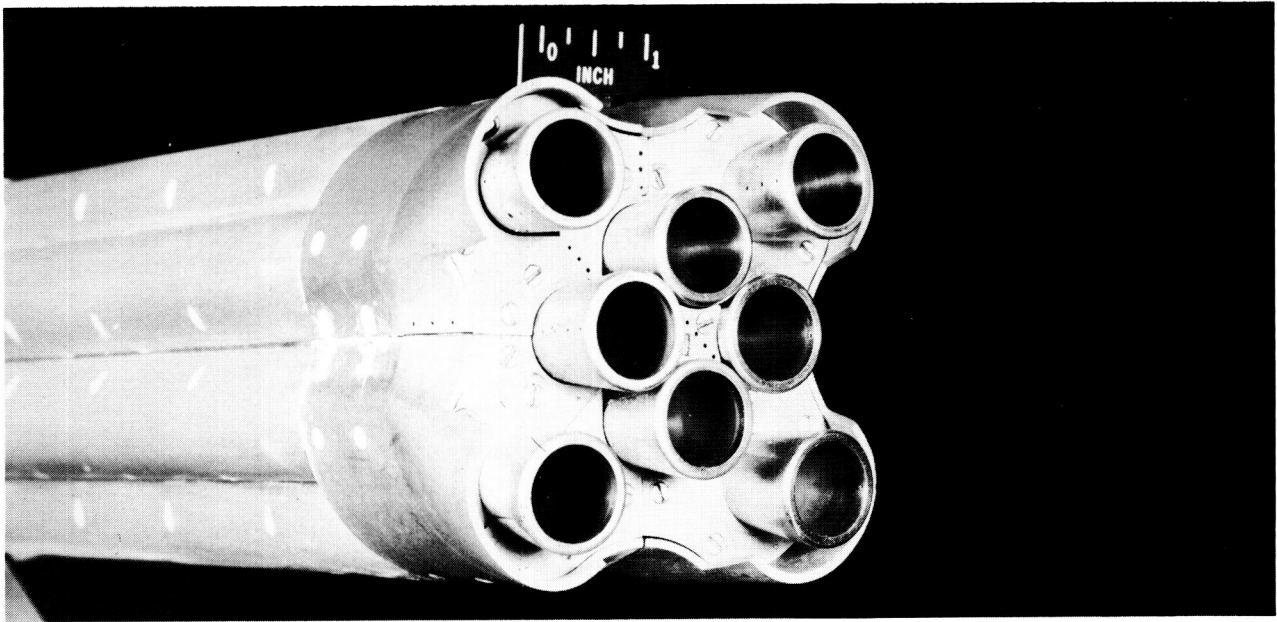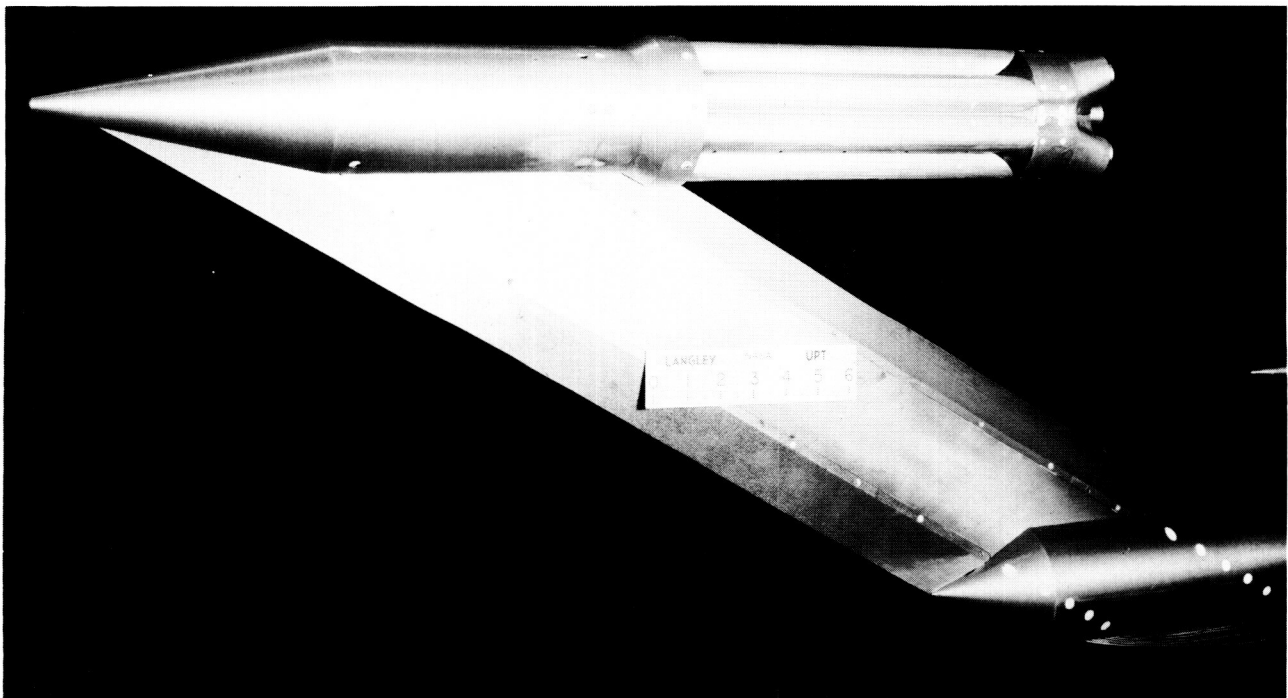|	Shroud
1	Basic shroud length; single flare.
2	Basic shroud length; double flare.
3	Shroud cut to heat shield.
4	Shroud cut to fire wall.
5	Pressure shroud (basic shroud length; single flare instrumented with 37 orifices).

**Range of α: 0°, -2°, -4°, and -8°.

Figure 1.- Tunnel installation of the C-1 Saturn model. (All dimensions in inches unless otherwise noted.)

11

Shroud cut to fire well
Shroud cut to heat shield
Basic shroud
(single and double flare)

Pressure tubes

Heat shield

SECTION A-A

Pressure tubes

30.5

10.581

1.011

0.701

4.062

3.424

8.035

6.965

5.447

12.48°

13.40°

.195R

1.250

6.372

18°

0.750 diam.
typical

1.625

14°

0.812

30°

(a) Drawing of C-1 Saturn model.

Figure 2.- Drawing and photograph of C-1 Saturn model used in nozzel hinge-moment tests. (All dimensions are in inches unless otherwise noted.)

L-61-7886

(b) Photographs of C-1 Saturn model with basic single-flare shroud.   L-61-7885

Figure 2.- Concluded.

Coordinates for Mach number 2.66 nozzle	
x	y
0	0.357
0.175	0.349
0.375	0.322
0.575	0.286
0.775	0.243
0.875	0.221
0.975	0.206
1.025	0.211
1.075	0.223
1.135	0.244
1.175	0.250
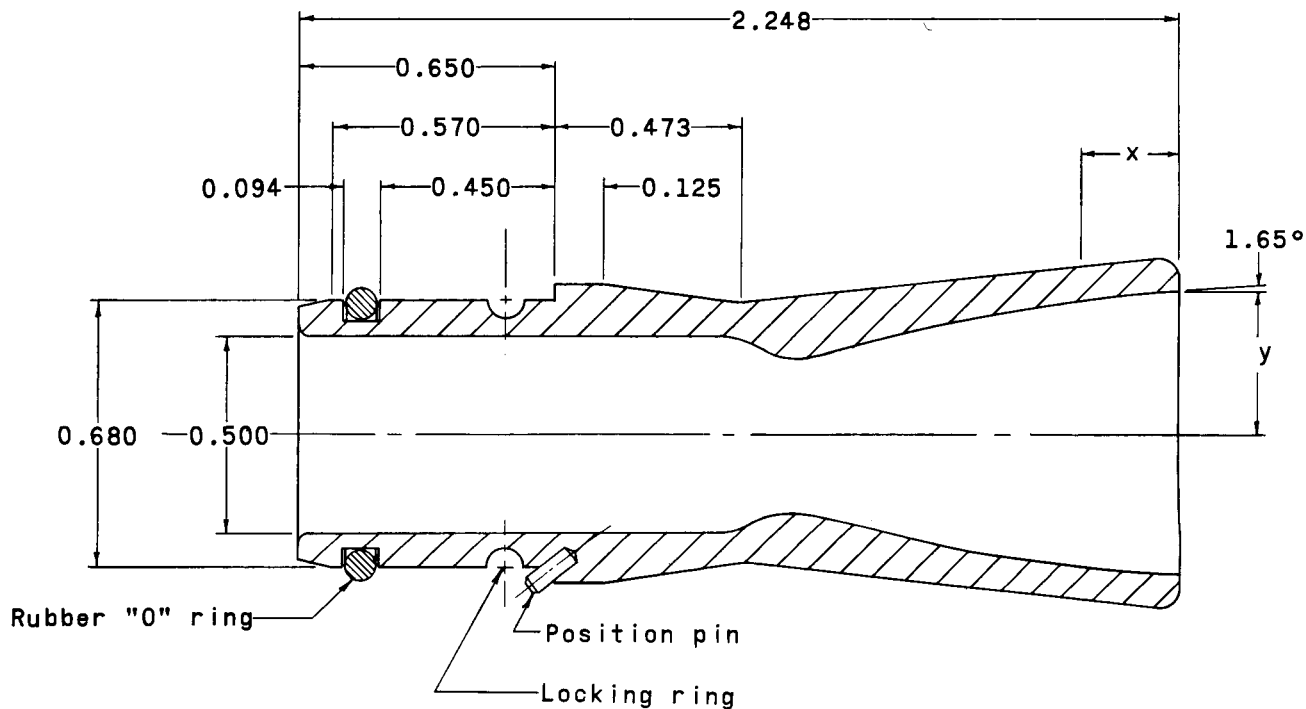
Note: All eight nozzles are identical.

Figure 3.- Details of nozzle. (All dimensions in inches unless otherwise noted.)

Orifice number	r, in.	φ, deg
63	0.230	135
64	.115	135
65	0	0
66	.115	315
67	.230	315
68	.681	315
69	.799	315
70	.917	315
71	1.126	0
72	1.251	0
73	1.376	0

Section A-A

Detail of heat shield between inboard nozzles.

Figure 4.- Orifice location on heat shields. (All dimensions are in inches unless otherwise indicated.)

Figure 5.- Orifice location on the nozzles.
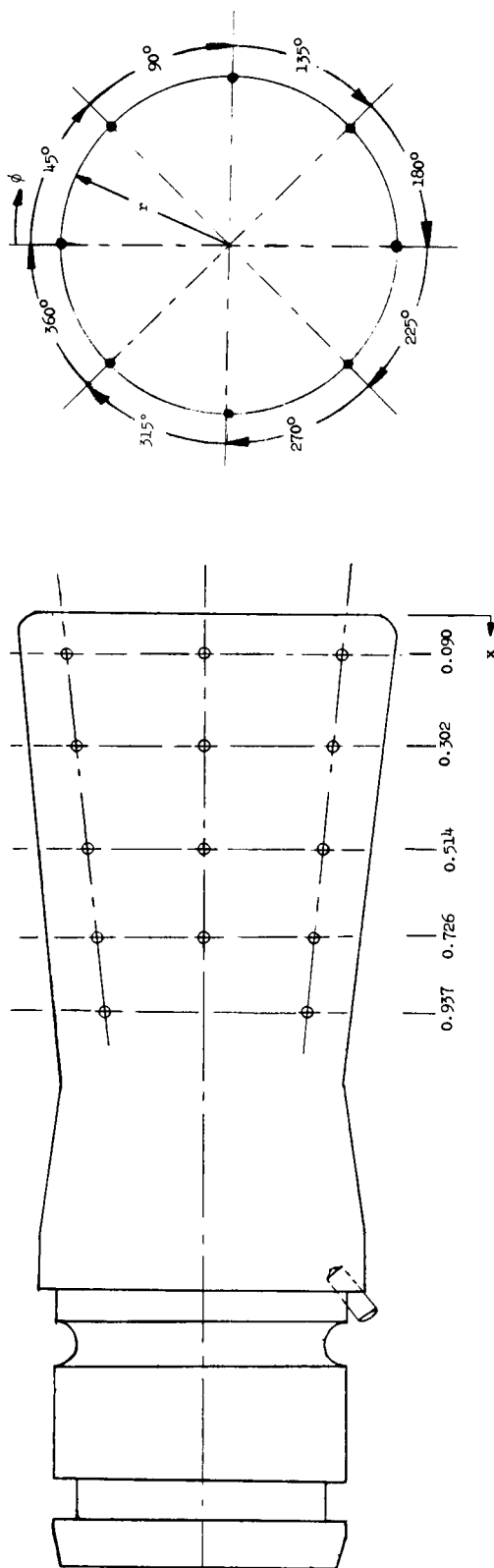
Nozzle number	x, in.	r, in.	ϕ, deg							
			0	45	90	135	180	225	270	315
2	0.090	0.445	1							8
	.302	.423	9	10	11	12	13	14	15	16
	.514	.395	17	18	19	20	21	22	23	24
	.726	.375	25		26			27		28
	.957	.368	29					30		
3	.090	.445	31	32	33		34		35	36
	.302	.423	37	38	39		40		41	42
	.514	.395	43		44		45		46	
	.726	.375	47				48			
	.957	.368	49				50			
6	.090	.445	51				52		53	
	.302	.423	54				55		56	
	.514	.395	57				58		59	
	.726	.375							60	
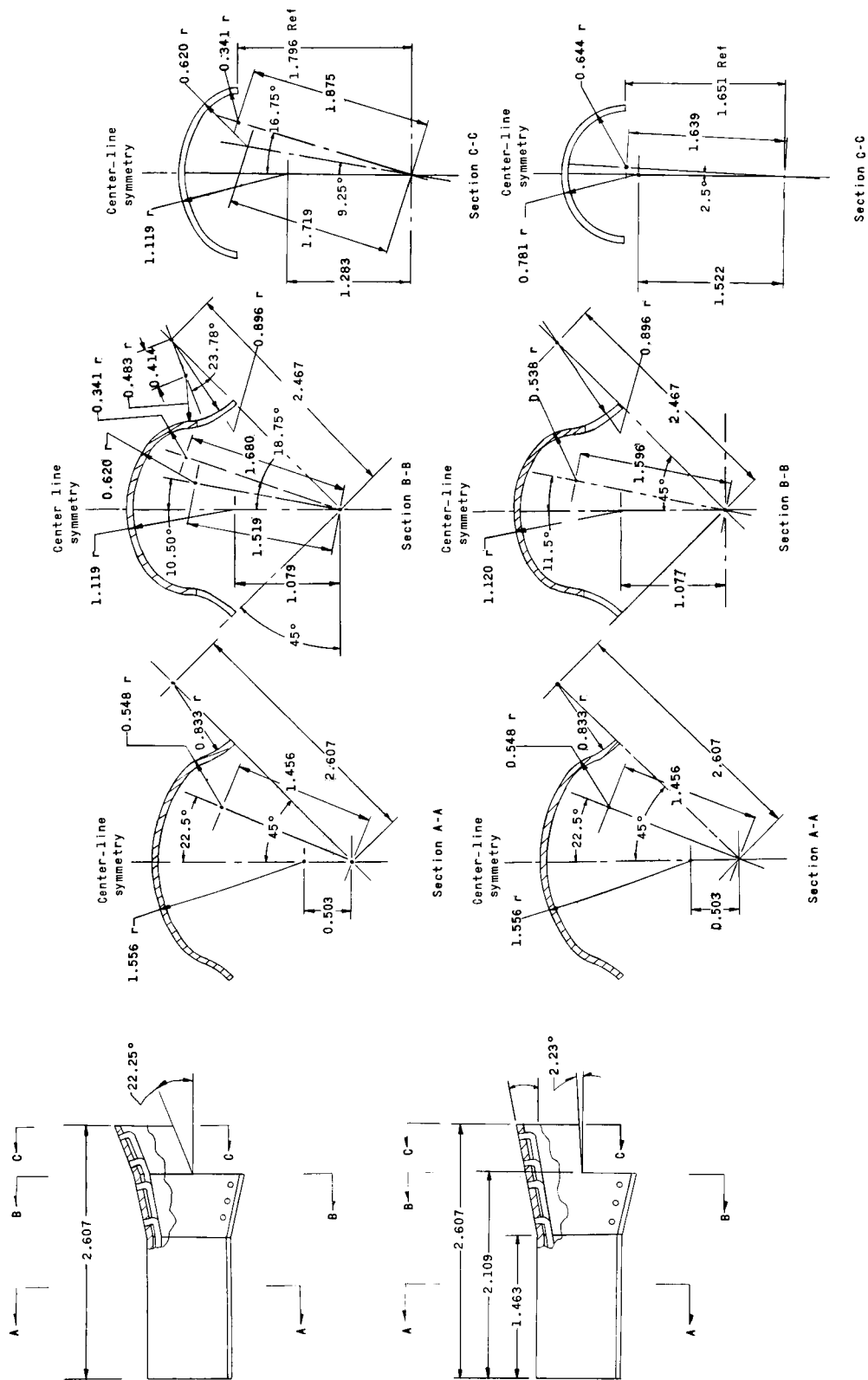
Figure 6.- Detail drawing of shrouds. (All dimensions in inches unless otherwise noted.)
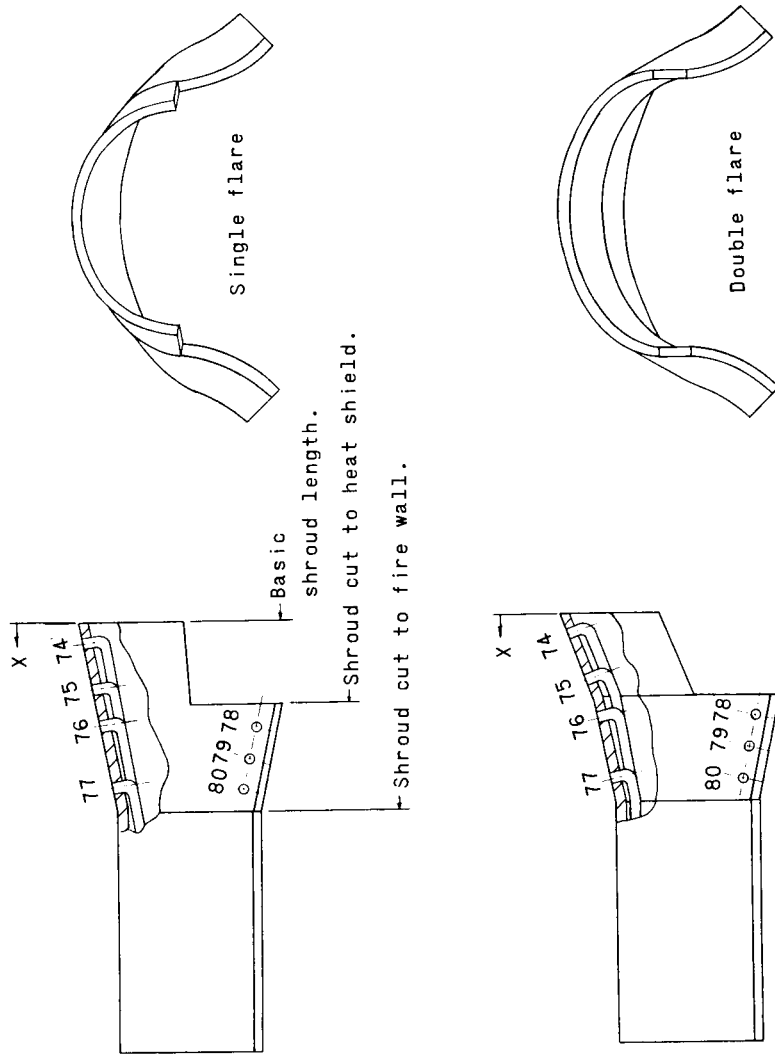
Shroud	Orifice Number	x, in.
Basic shroud length;single flare	74	0.125
	75	0.406
	76, 78	0.623
	79	0.811
	77, 80	0.998
Basic shroud length;double flare	74	0.125
	75	0.406
	76, 78	0.623
	79	0.811
	77, 80	0.998
Shroud cut to heat shield	76, 78	0.623
	79	0.811
	77, 80	0.998
Shroud cut to fire wall	none	

Figure 7.- Orifice locations on the shrouds.

87.70°
78.25°
67.50°
52.25°
45.00°
32.75°
22.75°
11.75°
2.75°

Shroud developed view

1.50
1.00
0.53
0.32
0.10

Y *→   1 2 3   4   5   6   7 8 9

0.37   0.10
         0.35   0.60   0.85   1.10

X

0.10

0.10

0.57

1.00
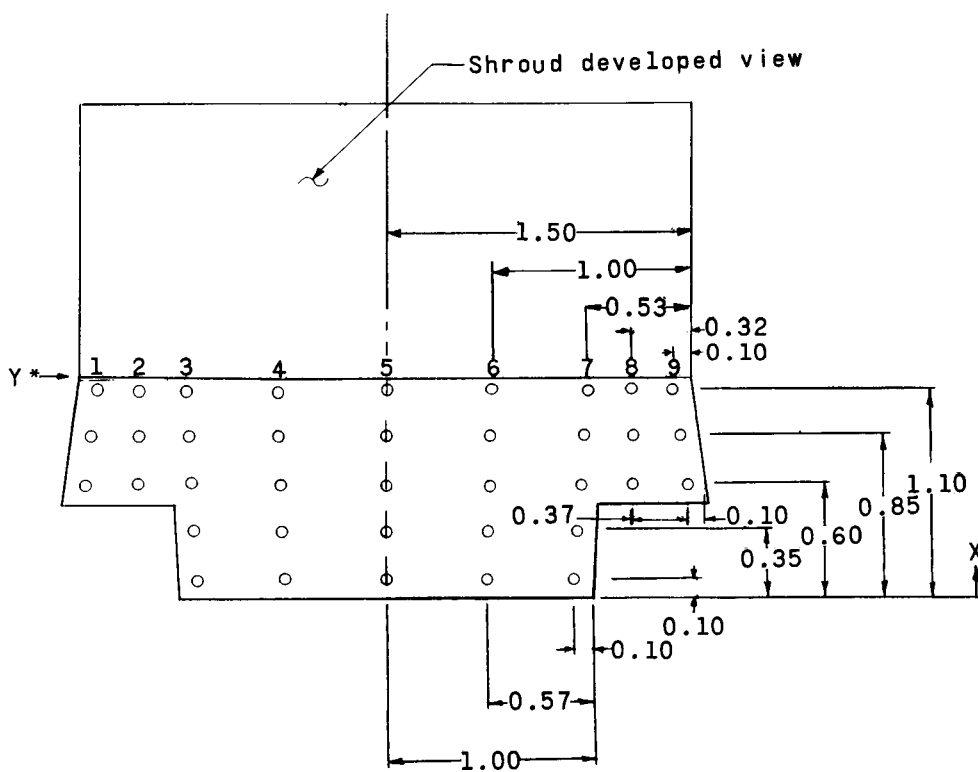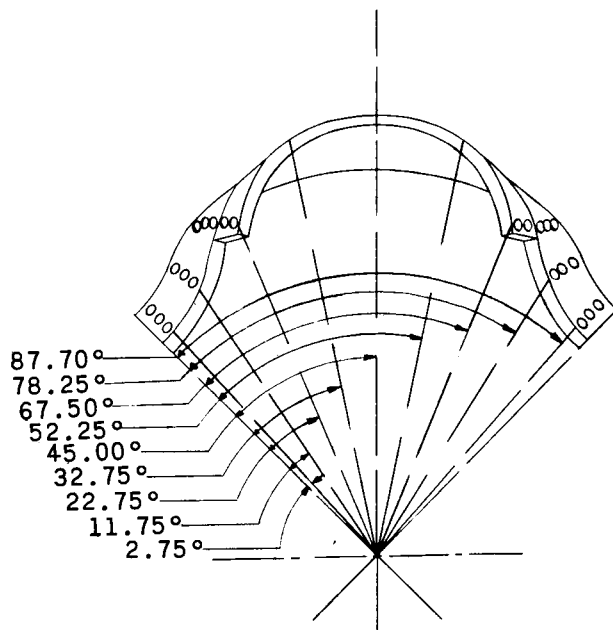
Figure 8.- Orifice locations on the single-flare special shroud.   (All dimensions are in inches unless otherwise stated.)
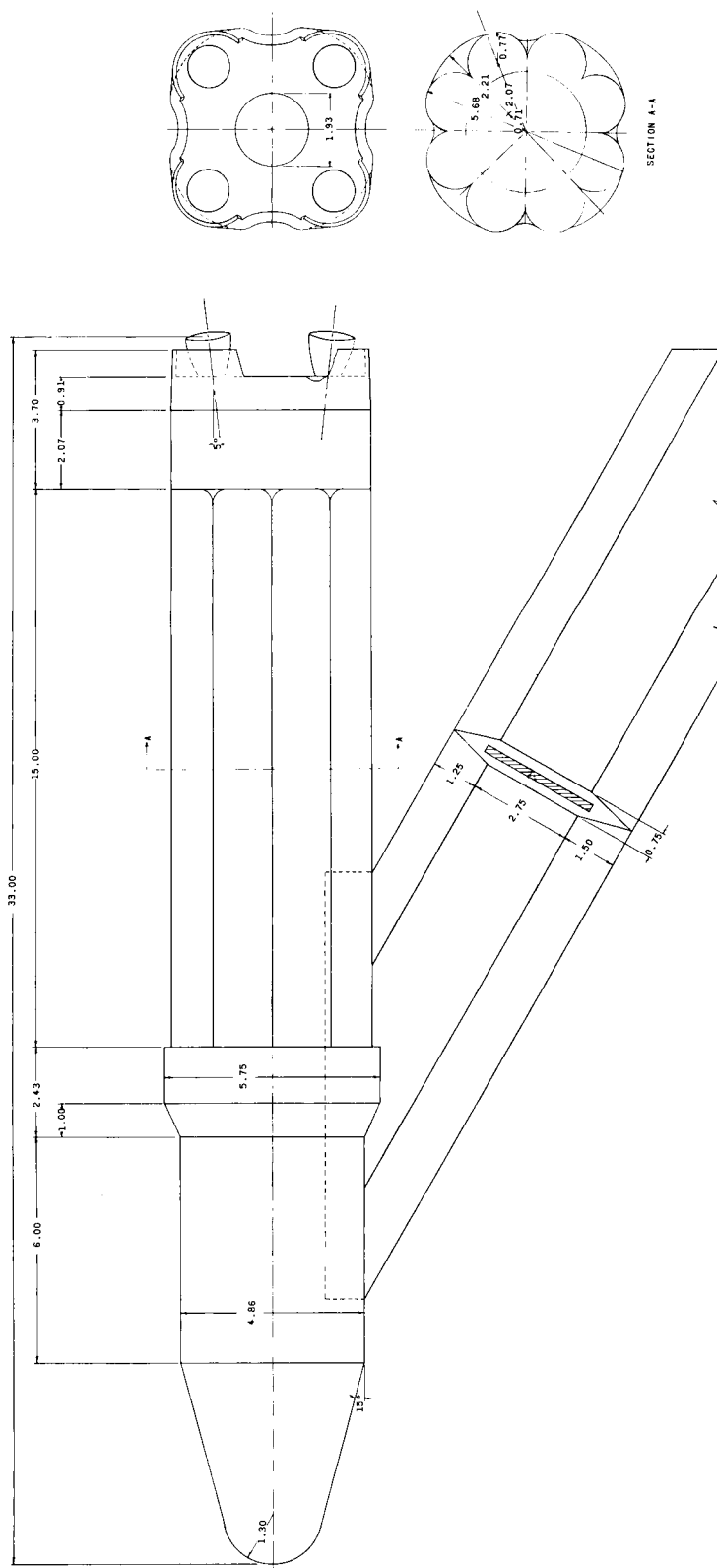
Figure 9.- Drawing of C-1 Saturn model used for strut interference tests. (All dimensions in inches unless otherwise noted.)
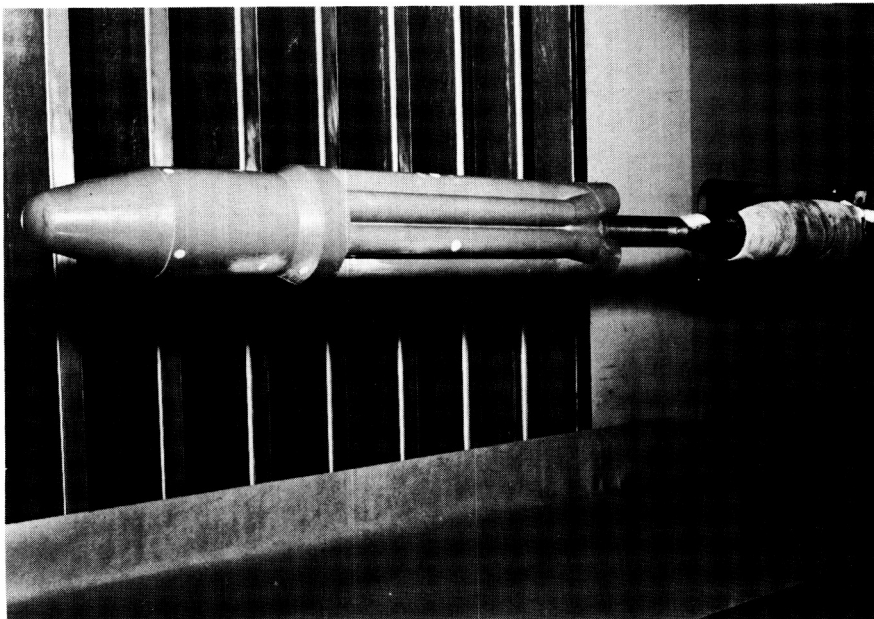
(a) Photograph of C-1 Saturn model with strut off.   L-60-7373
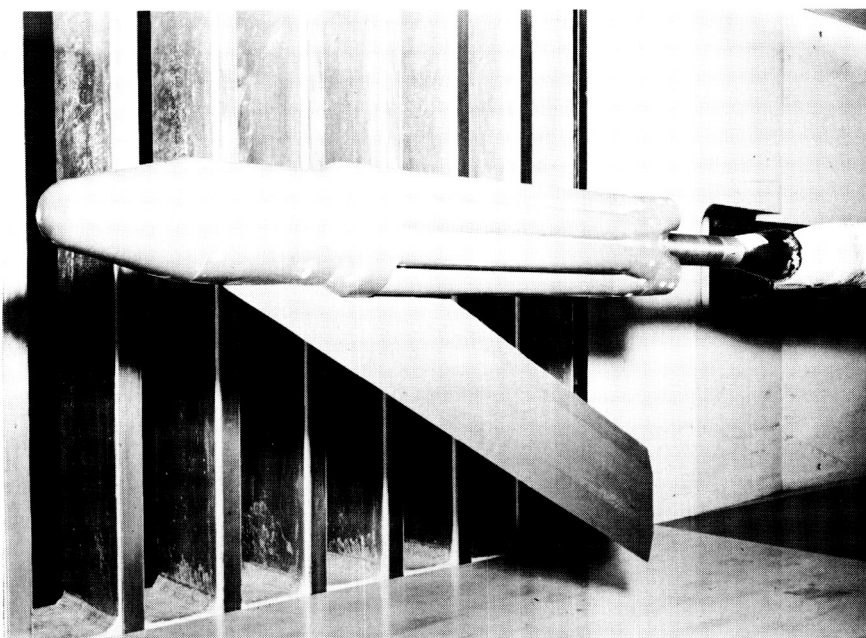
(b) Photograph of C-1 Saturn model with strut on.   L-60-7377

Figure 10.- Photographs of strut-interference model.

ANGLE φ

Location	x,in. r,in.	0°	22.5°	45.0°	67.5°	90.0°	180.0°	202.5°	225.0°	247.5°	270.0°	292.5°	315.0°	337.5°
Nozzle 1	0.43	17				18	19				20			
	1.07	21				22	23				24			
Nozzle 2	0.10	1				2	3				4			
	0.76	5				6	7				8			
Nozzle 3	0.10	9				10	11				12			
	0.76	13				14	15				16			
Nozzle 4	0.43	25				26	27				28			
	1.07	29				30	31				32			
After-body	0.10	47					48		45				46	
	1.22	52				56	57	58	49	60	50	62	51	
	2.72		53	54	55				59		61		63	64
Base	1.4	33					34				35			
	2.0	36					37	38	43	39	40	41	44	42
	2.8													
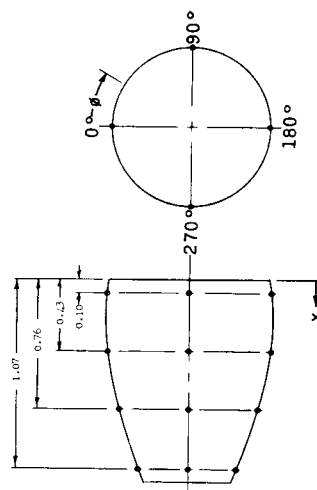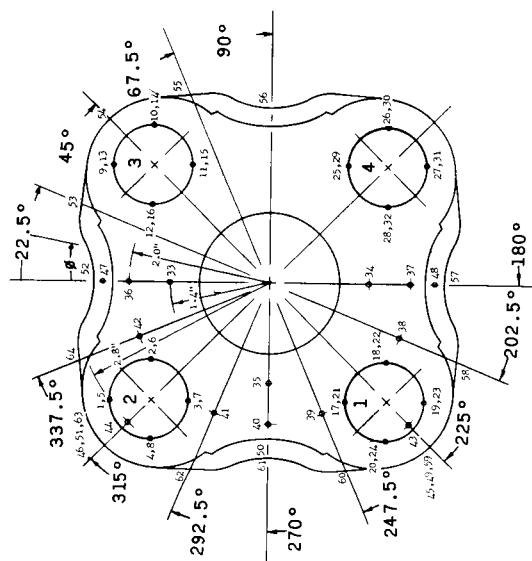
All possible orifice locations

Figure 11.- Pressure orifice location on C-1 Saturn strut-interference model.
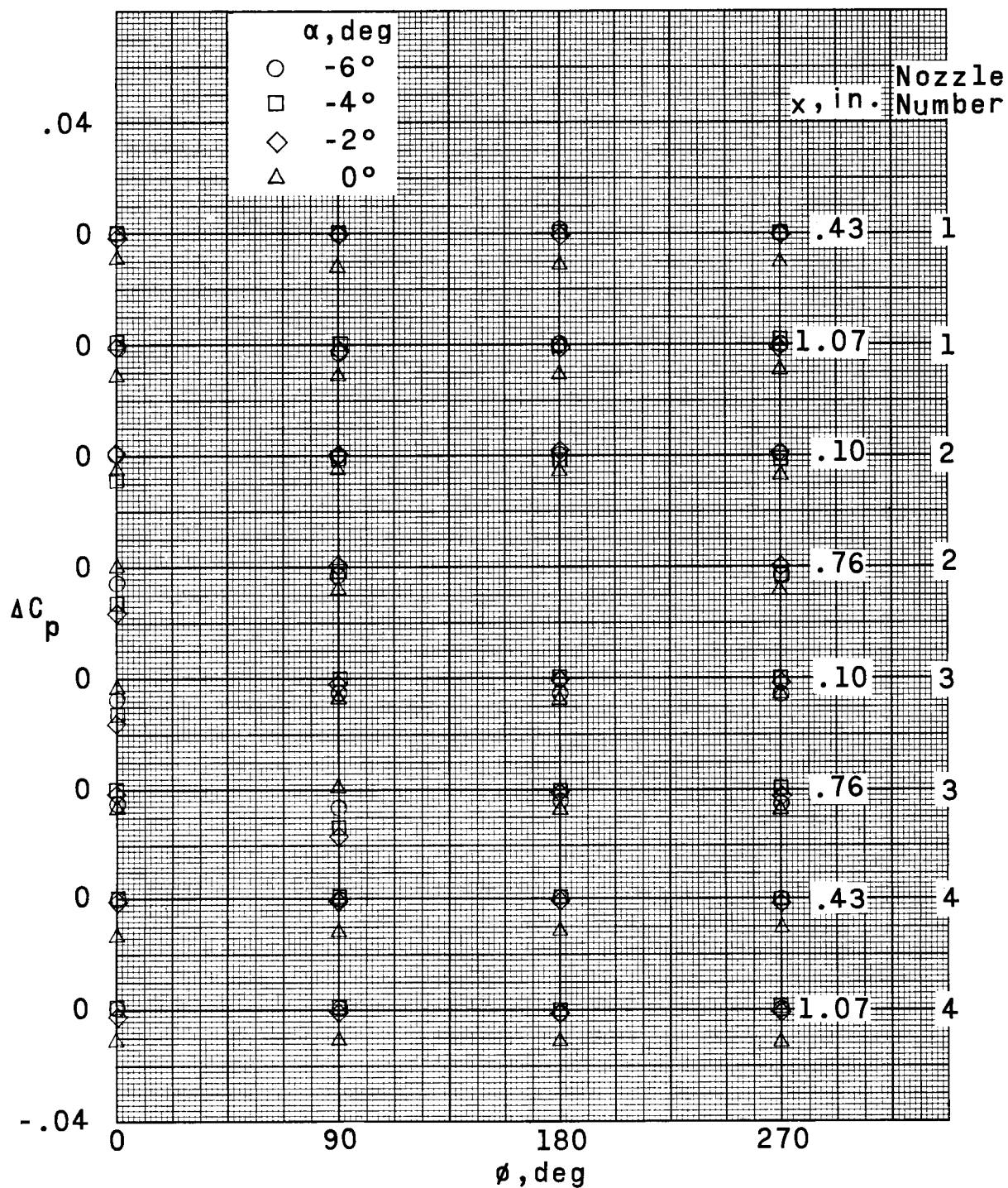
(a) $M_\infty = 1.60$.

Figure 12.- Effects of strut on the pressure of the four outer nozzles of C-1 Saturn vehicle at various Mach numbers.
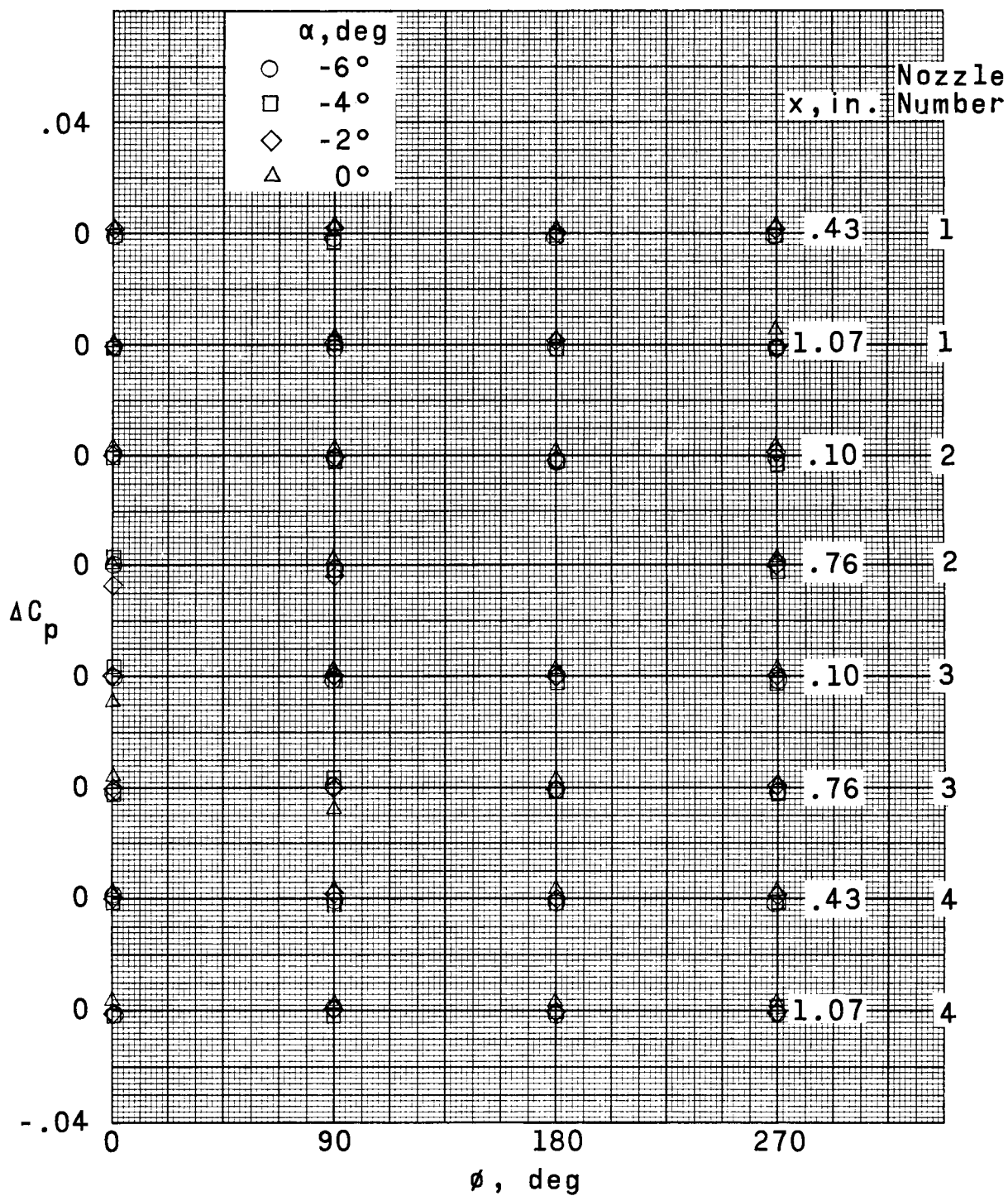
(b) $M_\infty = 2.00.$

Figure 12.- Continued.
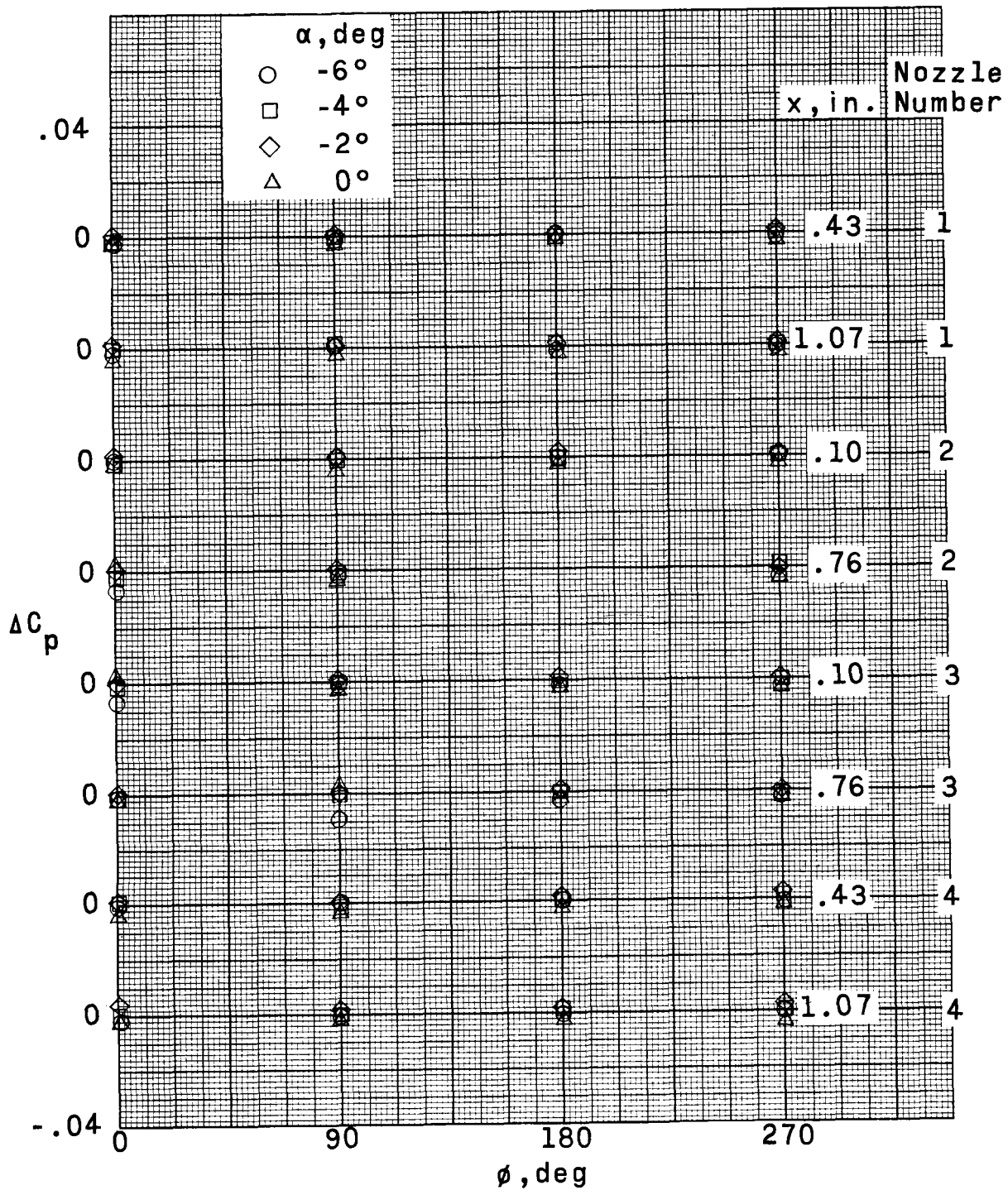
(c) $M_\infty = 2.50$.

Figure 12.- Continued.
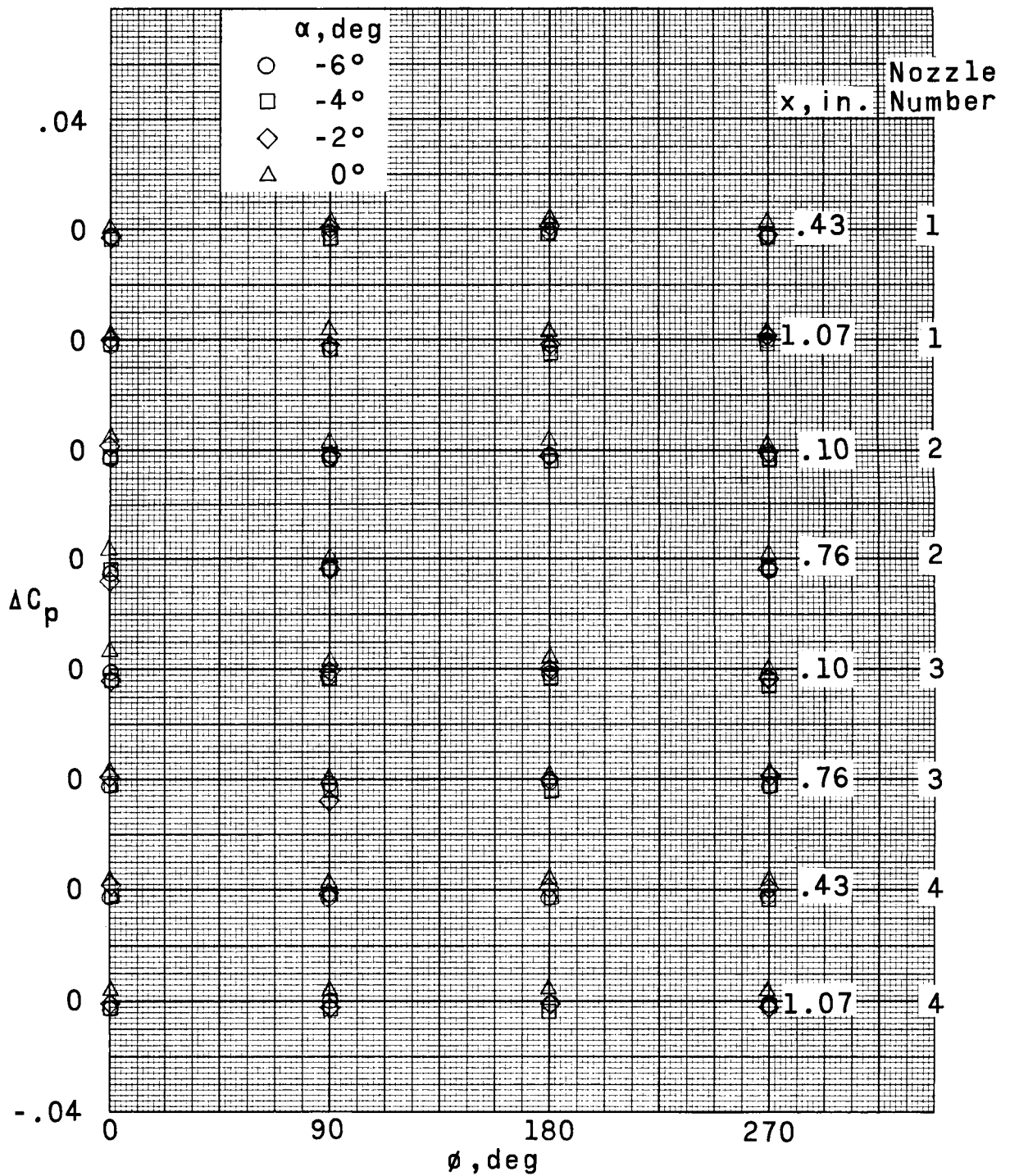
(d) $M_\infty = 2.80$.

Figure 12.- Concluded.
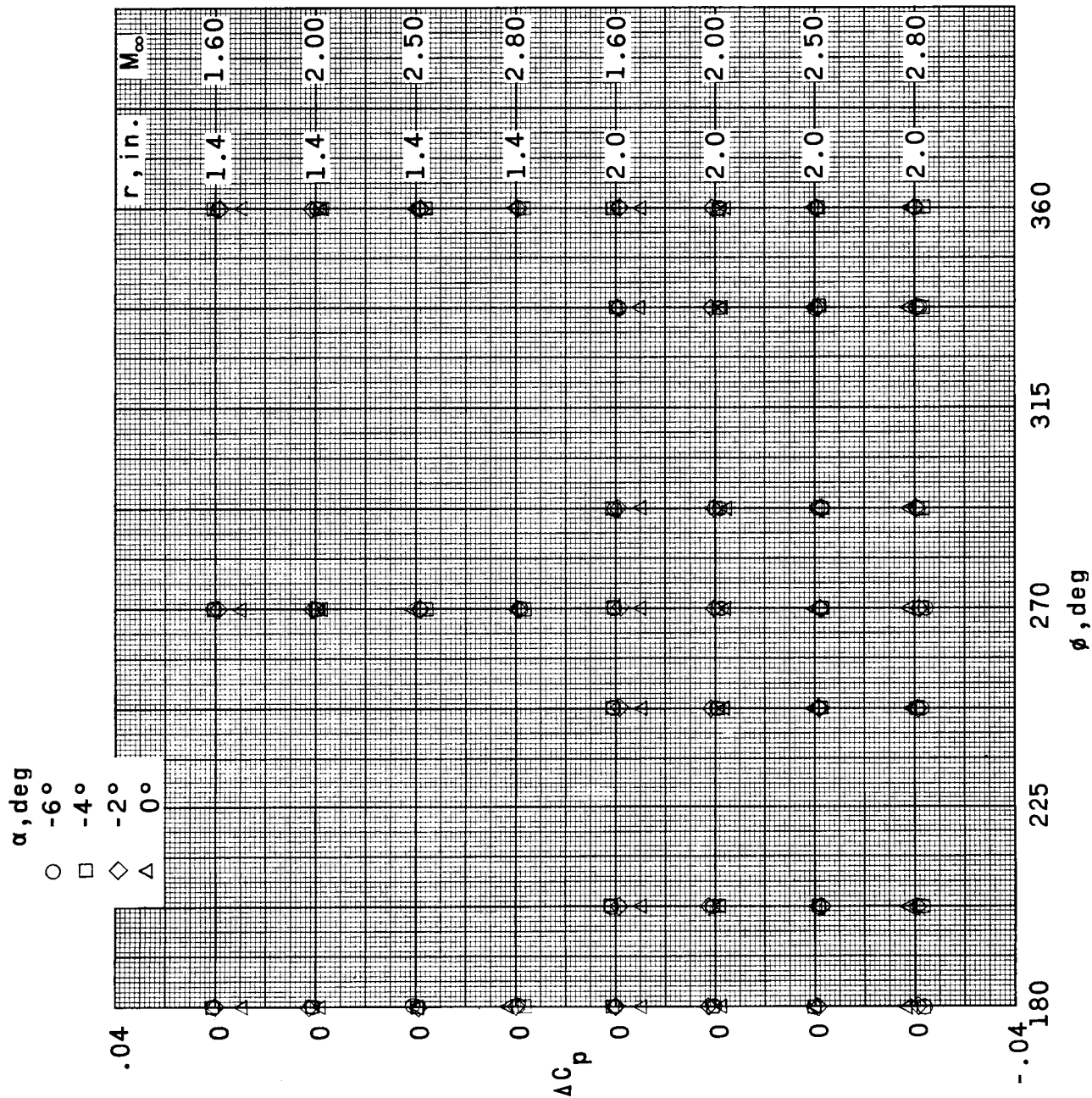
Figure 13.- Effects of strut on the base pressures of the C-1 Saturn vehicle.
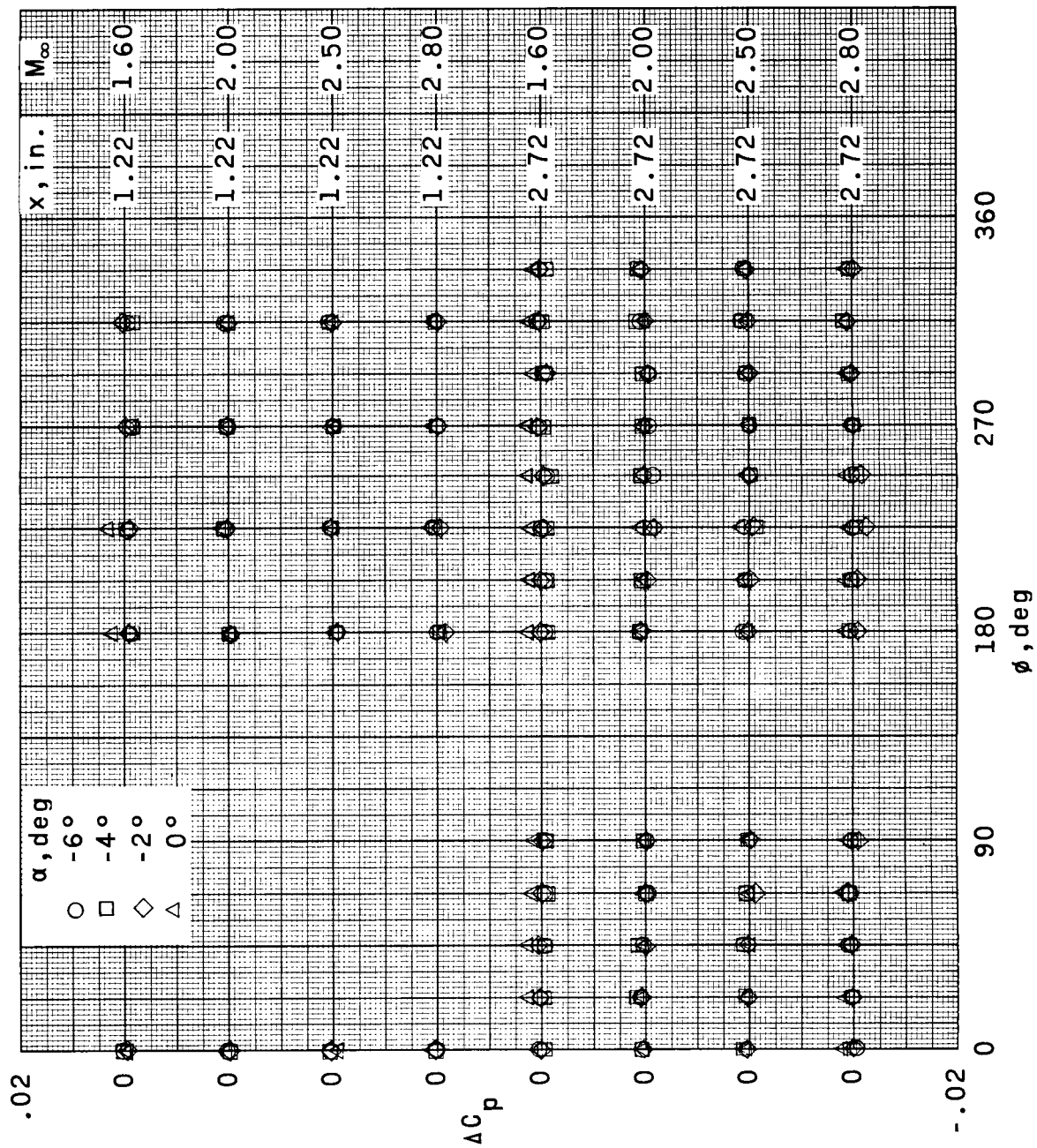
Figure 14.- Effects of strut on the shroud and afterbody pressures of the C-1 Saturn vehicle.

28
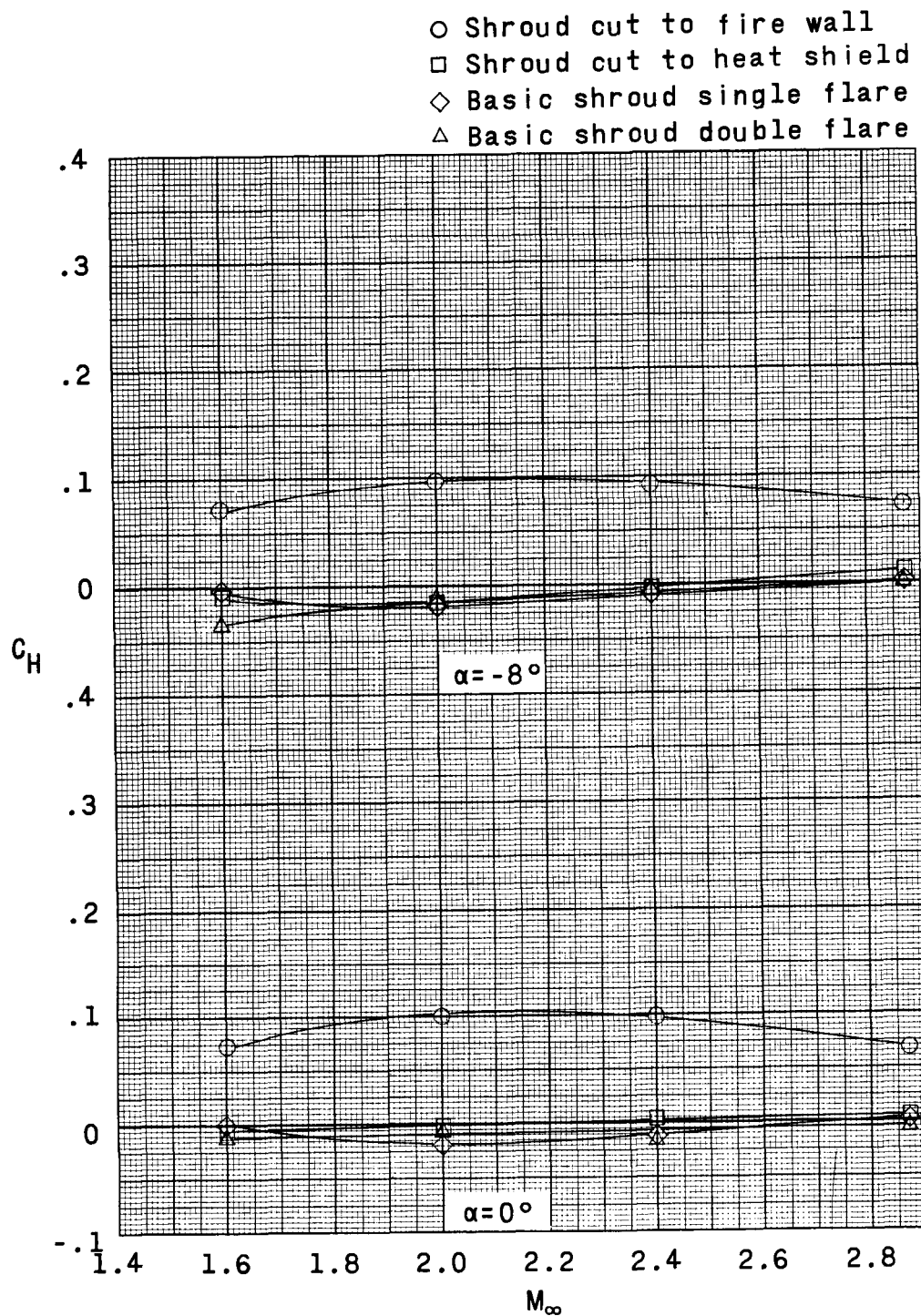
Figure 15.- Effect of shroud geometry on the variation of nozzle hinge-moment coefficient with Mach number. Jet off.

(a) $\delta_n = -3°$.

○ Shroud cut to fire wall
□ Shroud cut to heat shield
◇ Basic shroud single flare
△ Basic shroud double flare

$\alpha = -8°$

$\alpha = 0°$

C_H

M_∞

(b) $\delta_n = 6°$.

Figure 15.- Continued.

○ Shroud cut to fire wall
□ Shroud cut to heat shield
◇ Basic shroud single flare
△ Basic shroud double flare

$\alpha = -8°$

$\alpha = 0°$

C_H

M_∞
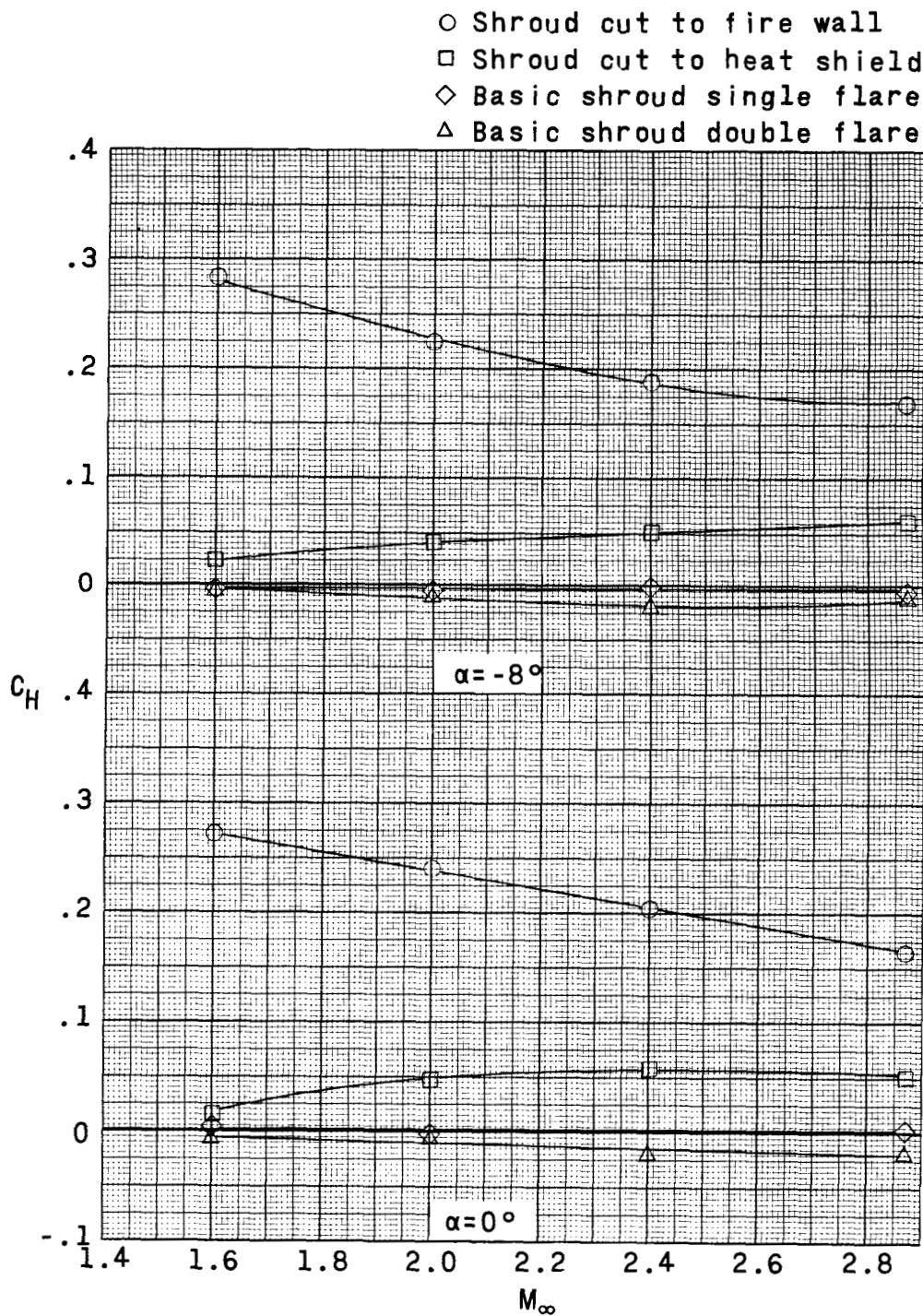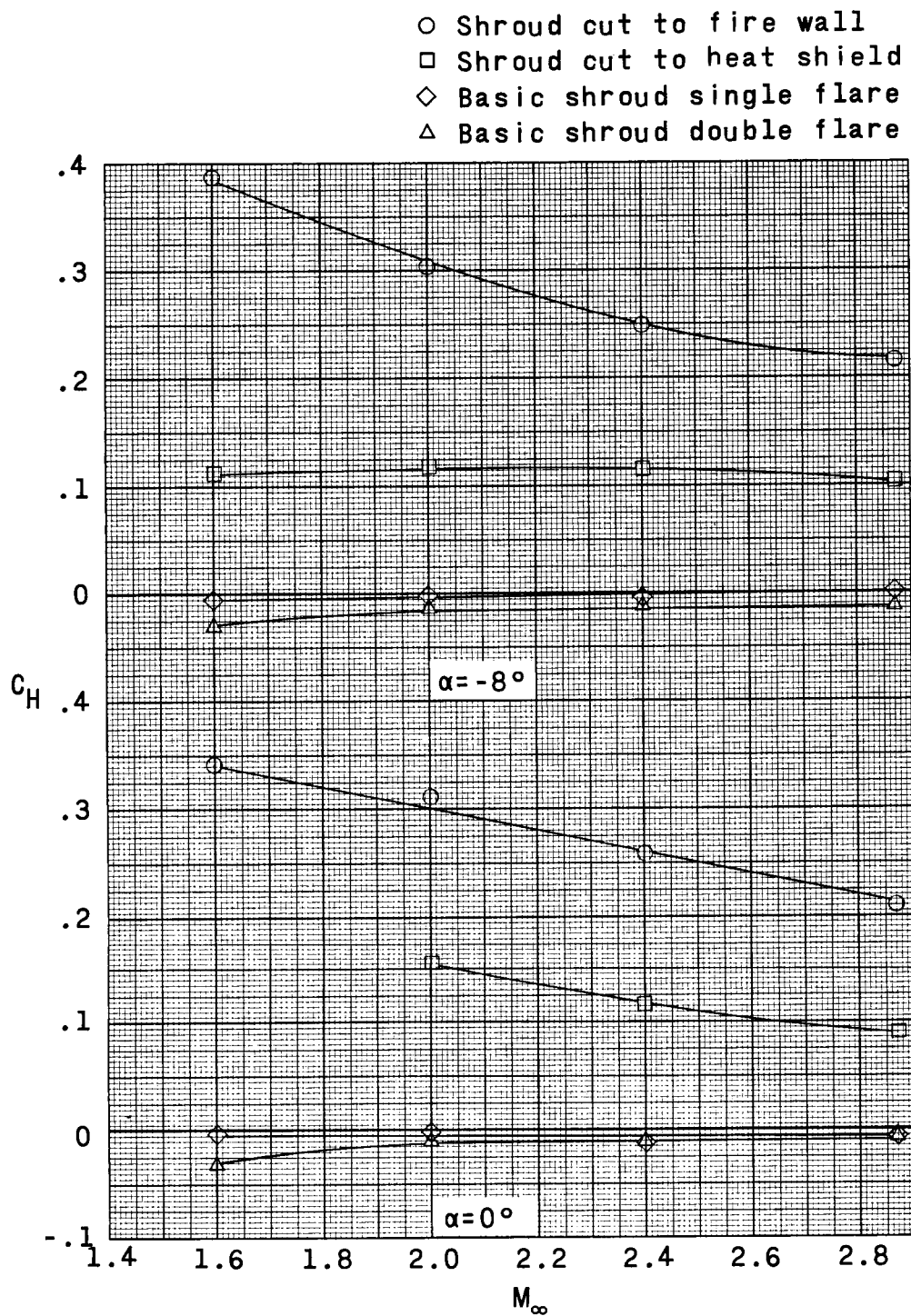
(c) $\delta_n = 12°$.

Figure 15.- Concluded.
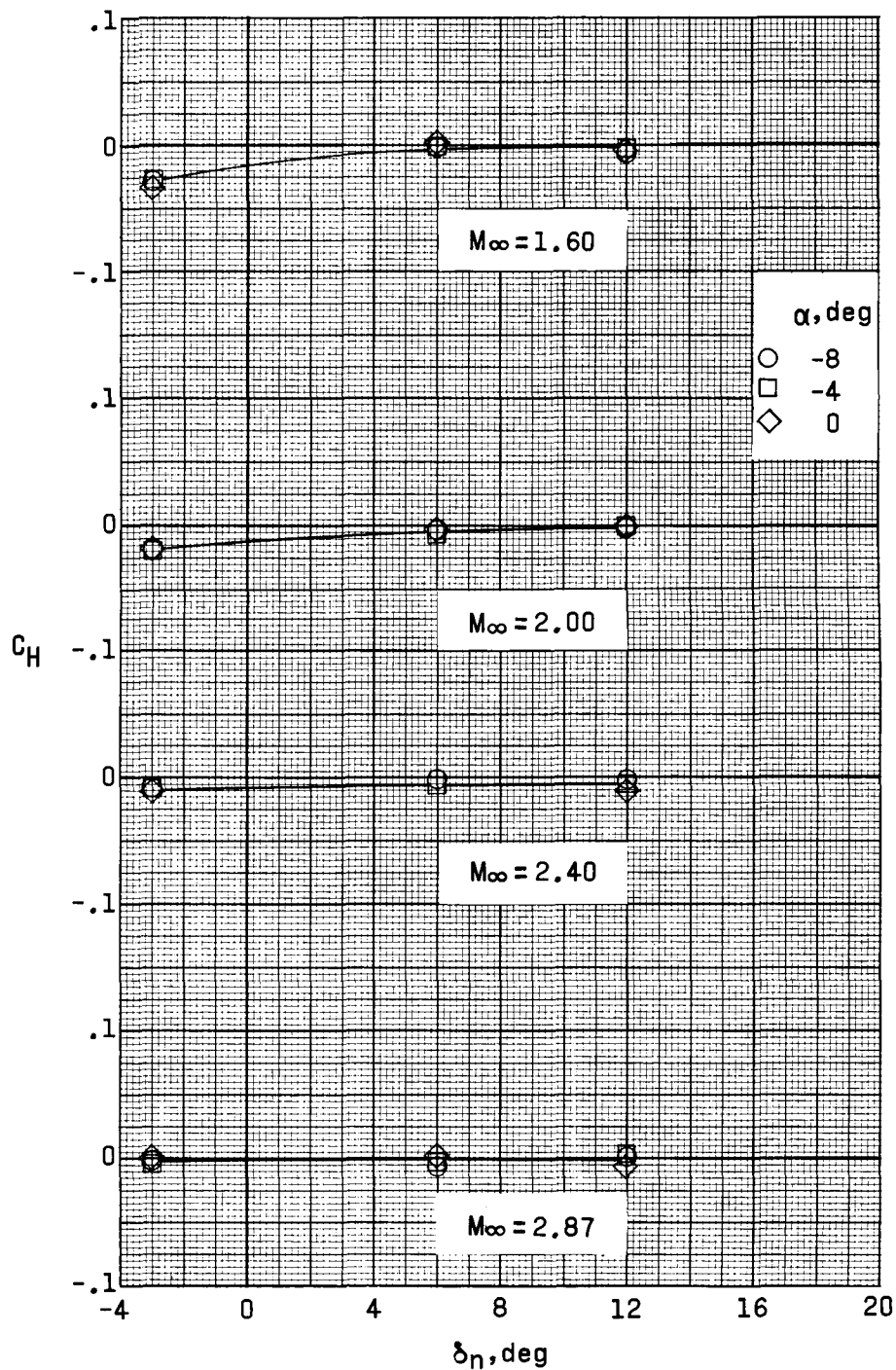
(a) Basic shroud length; single flare.

Figure 16.- Effect of angle of attack on the variation of nozzle hinge-moment coefficient with gimbal angle. Jet off.
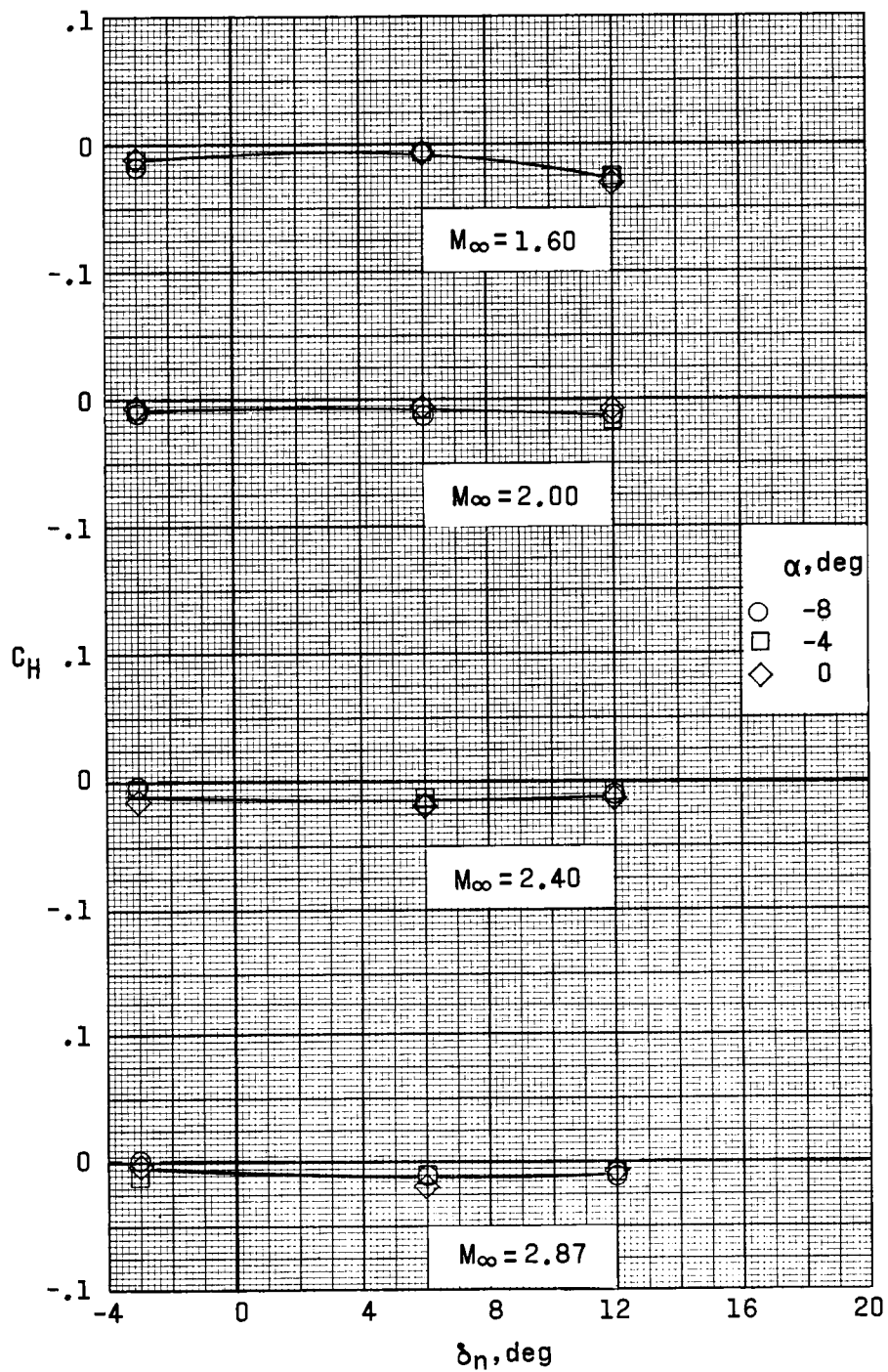
(b) Basic shroud length; double flare.

Figure 16.- Continued.
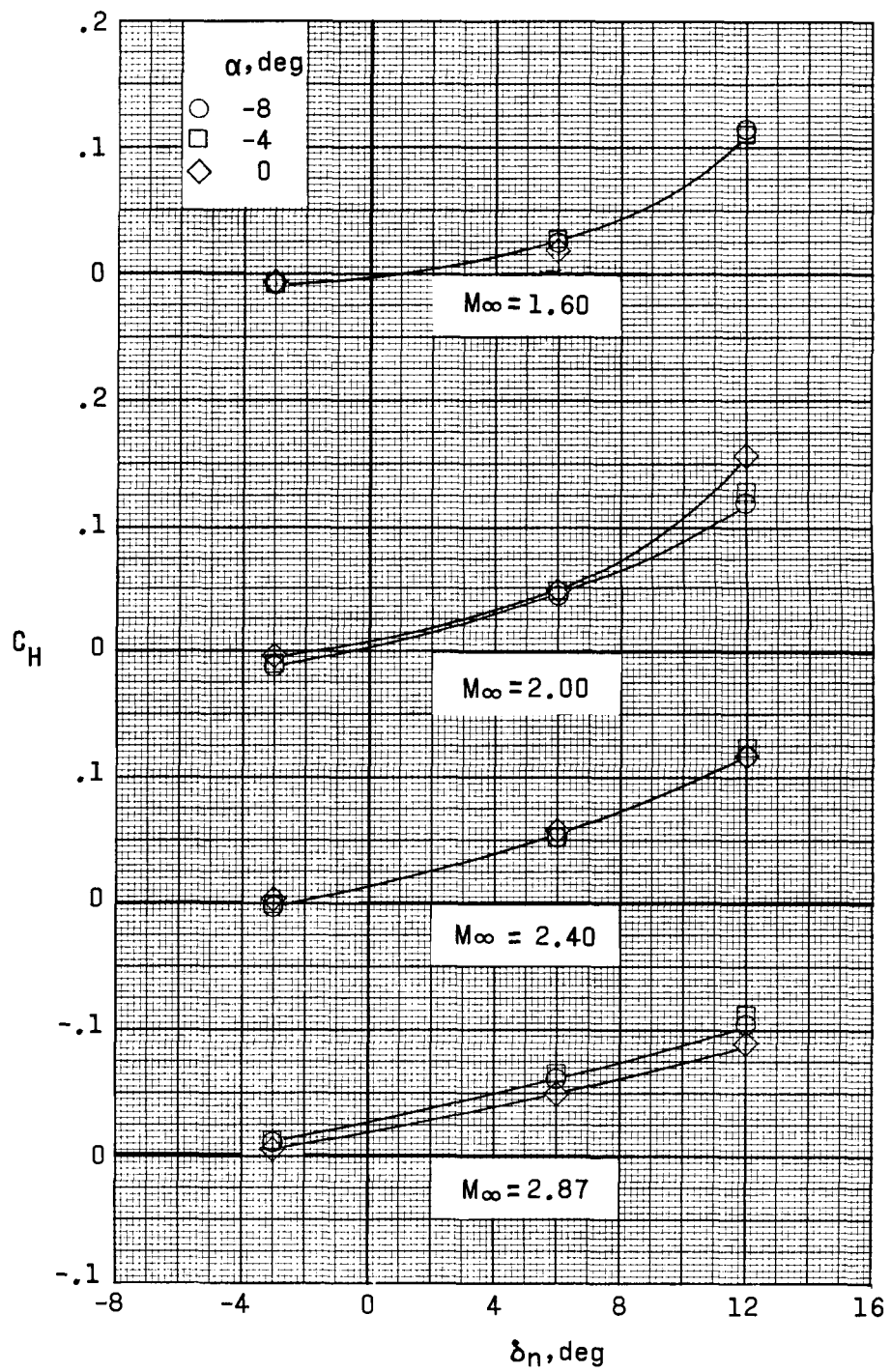
(c) Shroud cut to heat shield.

Figure 16.- Continued.
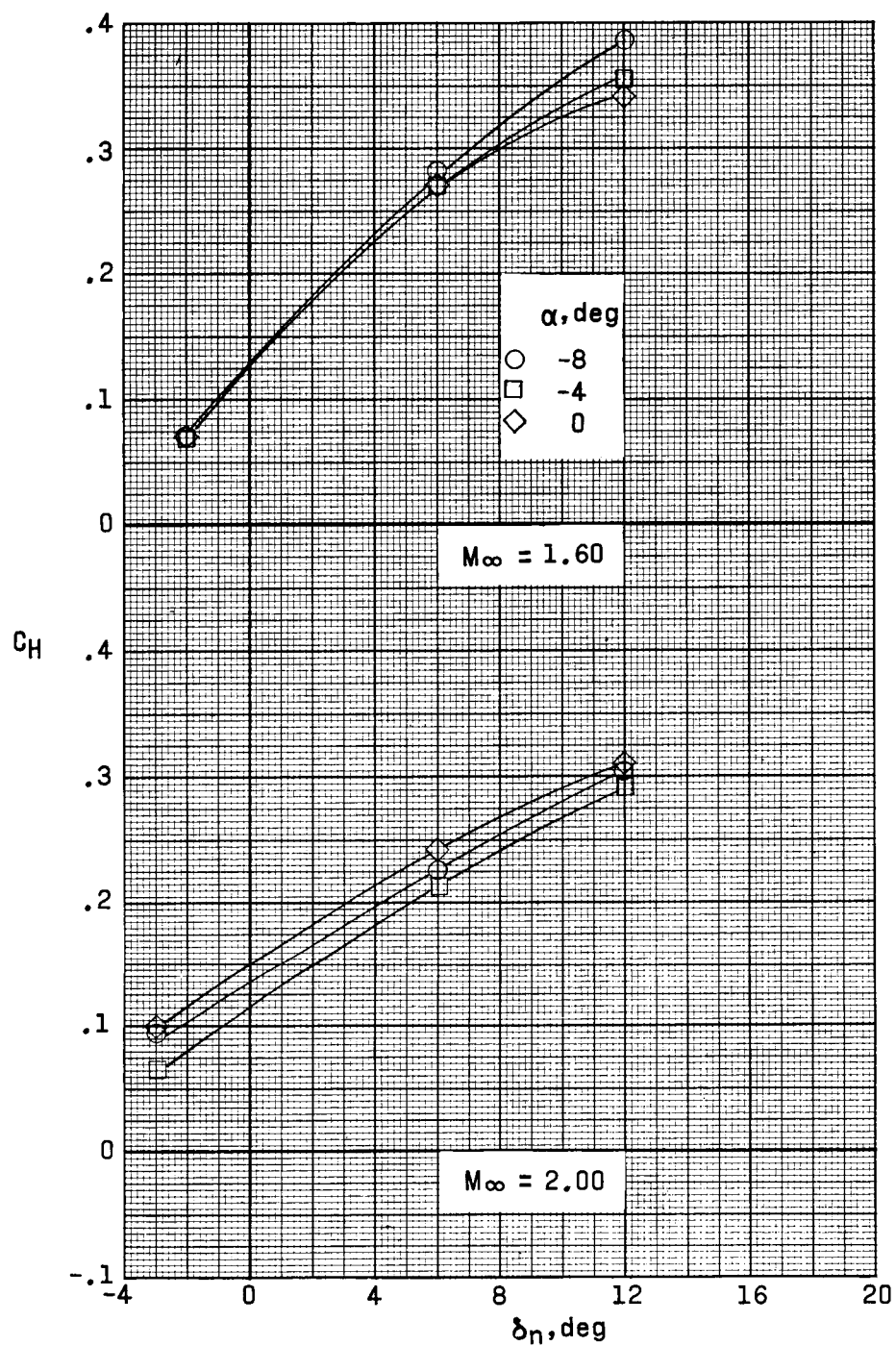
(d) Shroud cut to fire wall.

Figure 16.- Continued.
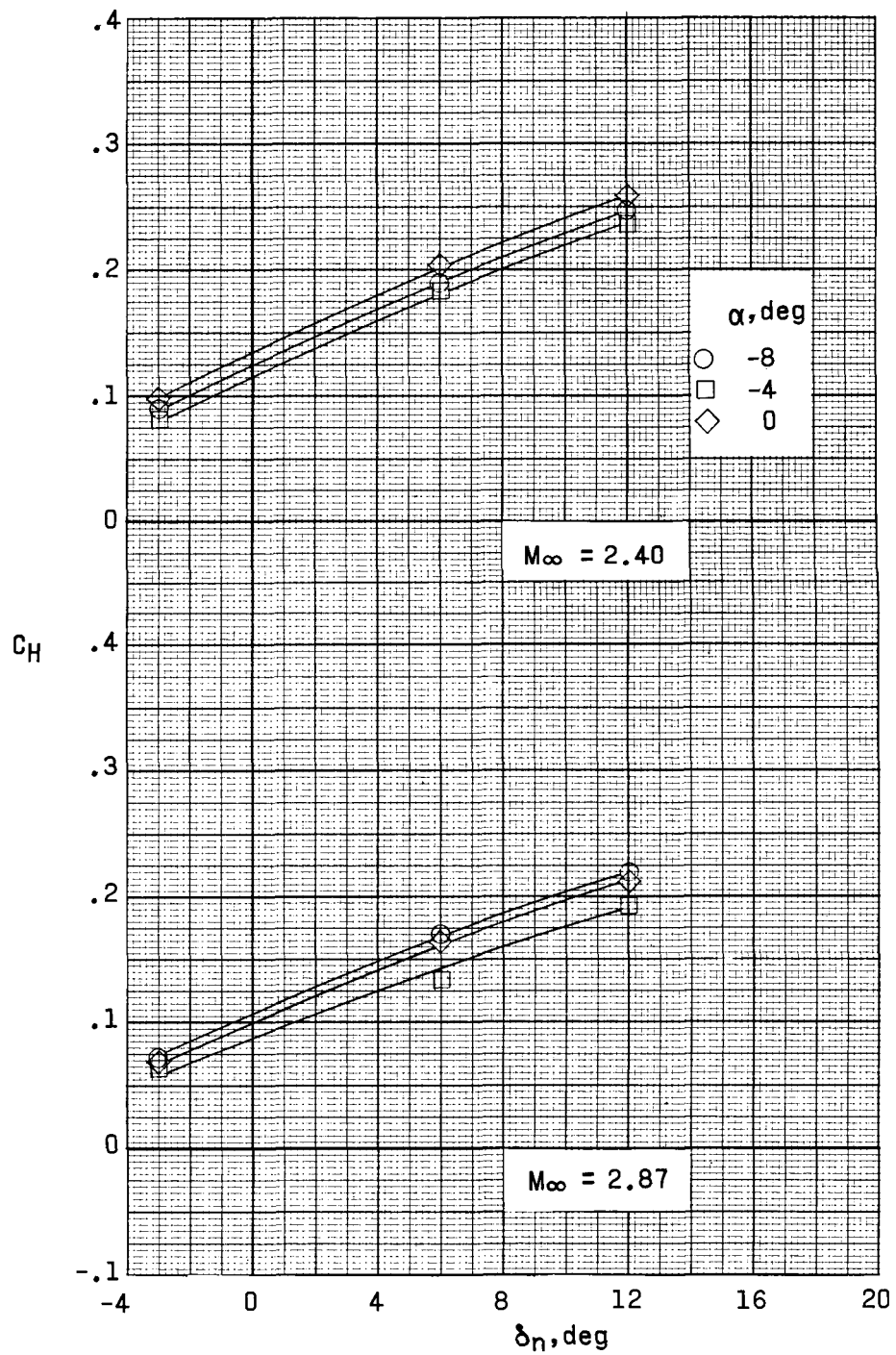
(d) Concluded.

Figure 16.- Concluded.
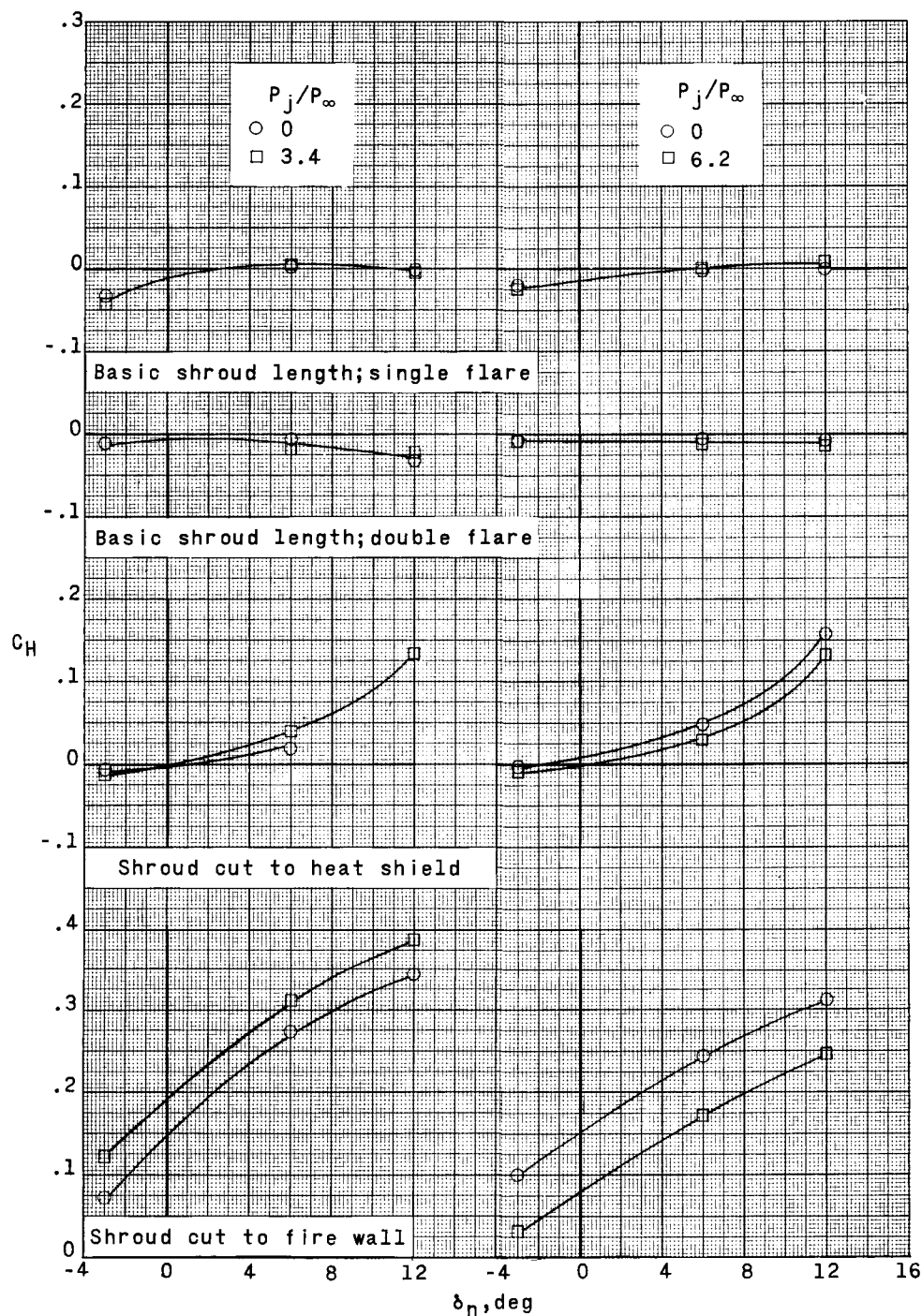
(a) M_∞ = 1.60.   (b) M_∞ = 2.00.

Figure 17.- Effect of jet pressure ratio on the variation of nozzle hinge-moment coefficient with gimbal angle. α = 0°.
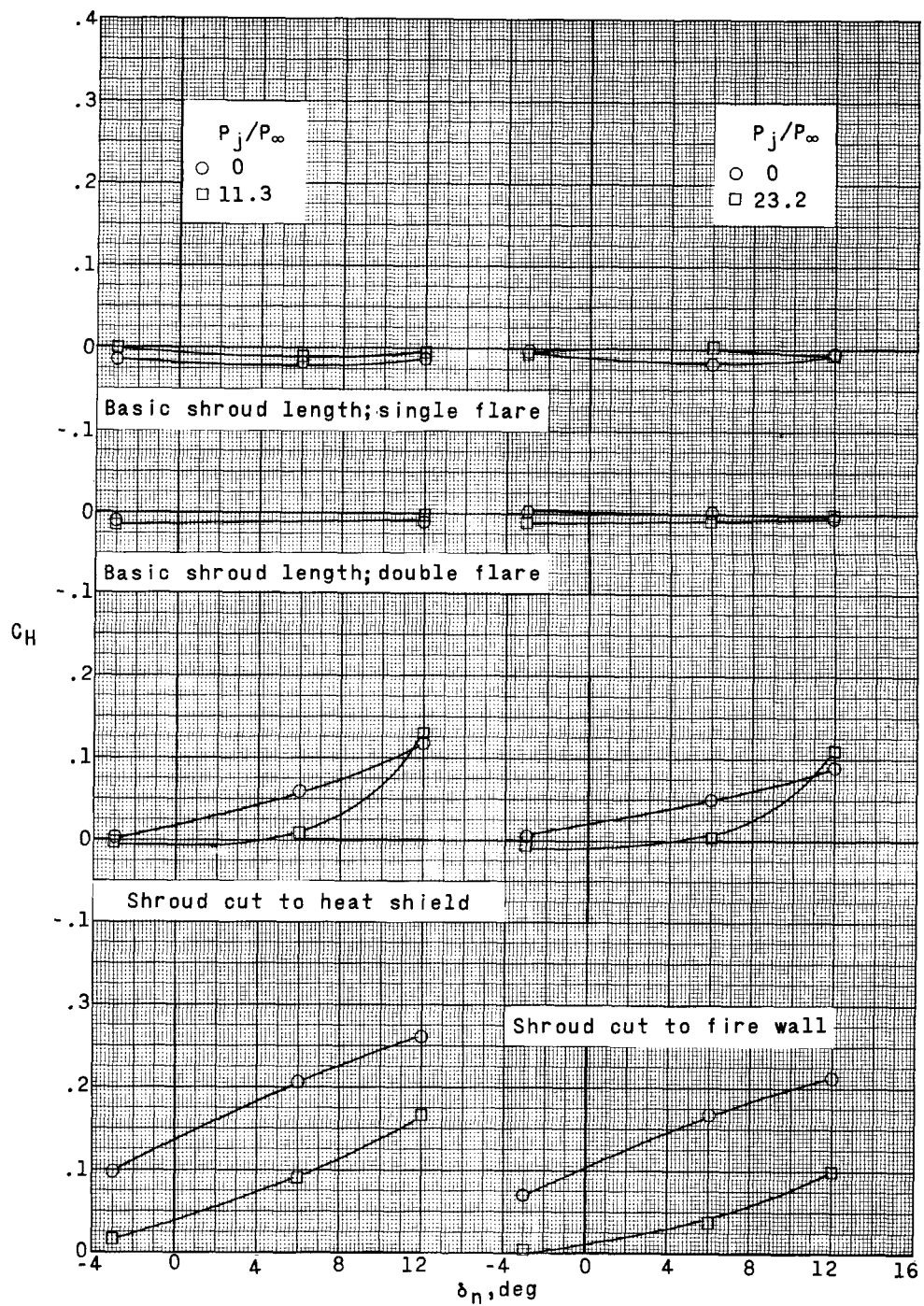
(c) $M_\infty = 2.40.$ (d) $M_\infty = 2.87.$

Figure 17.- Concluded.
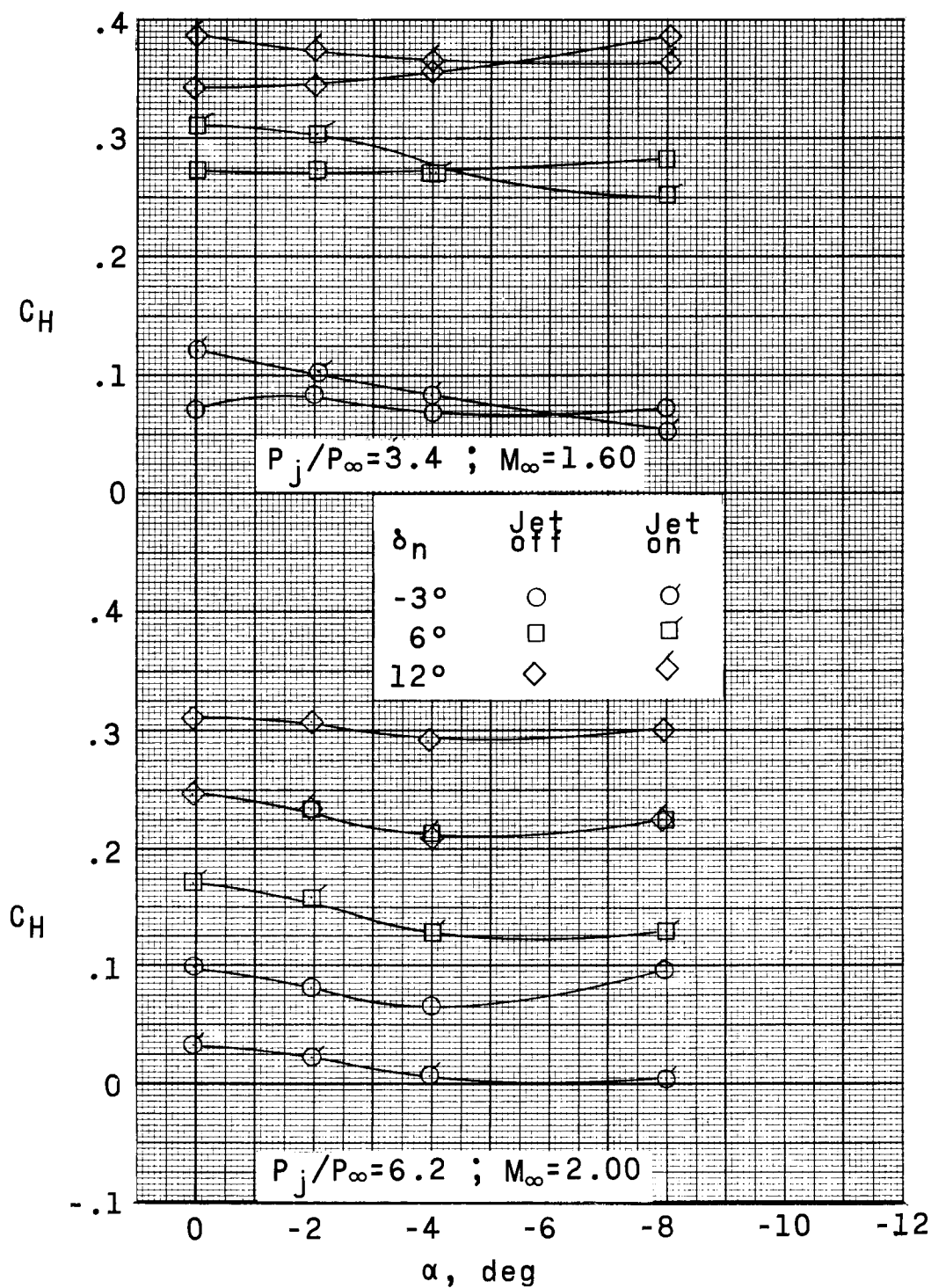
Figure 18.- Effect of jet pressure ratio on the variation of nozzle hinge-moment coefficient with angle of attack with shroud cut to fire wall.
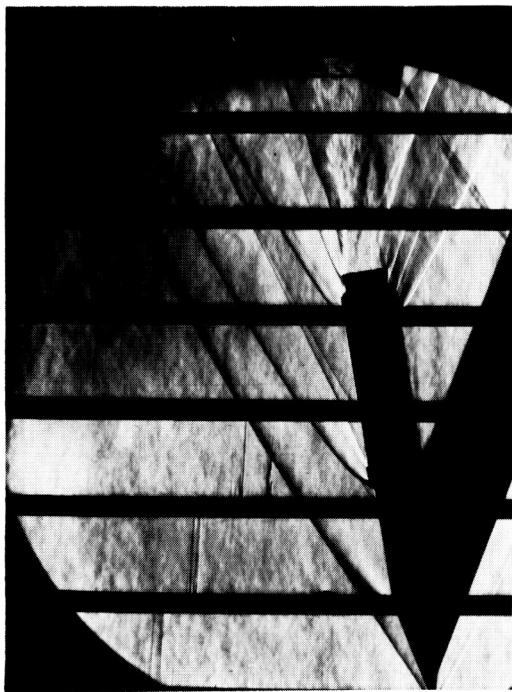
$p_j/p_\infty = 11.4$; $M_\infty = 2.40$
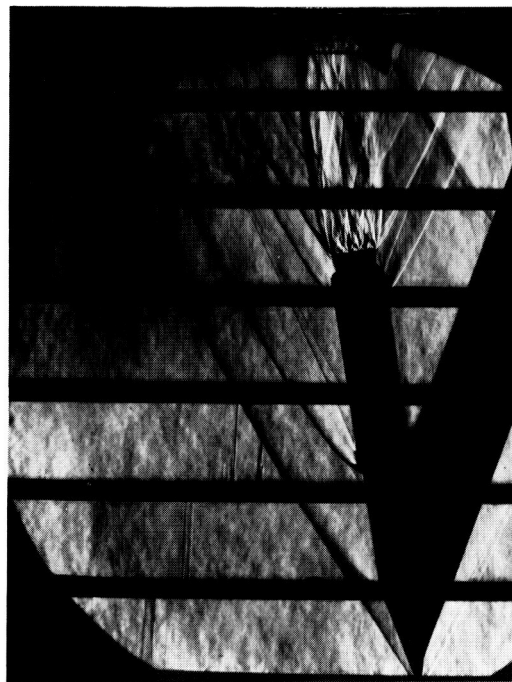
$p_j/p_\infty = 23.2$; $M_\infty = 2.87$

$p_j/p_\infty = 0$; $M_\infty = 2.40$
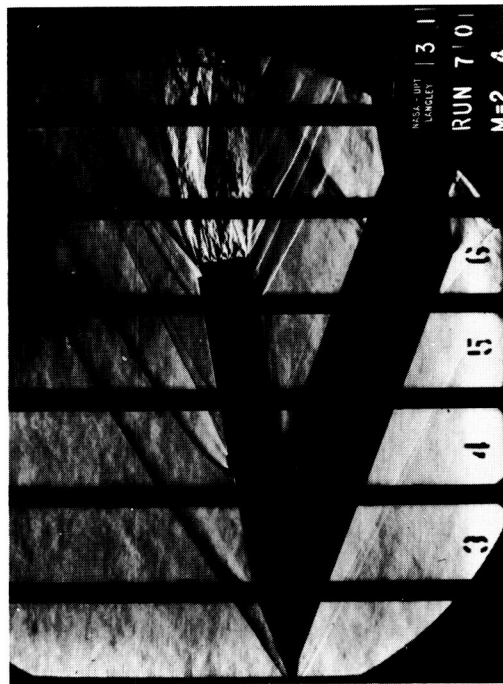
$p_j/p_\infty = 6.2$; $M_\infty = 2.00$
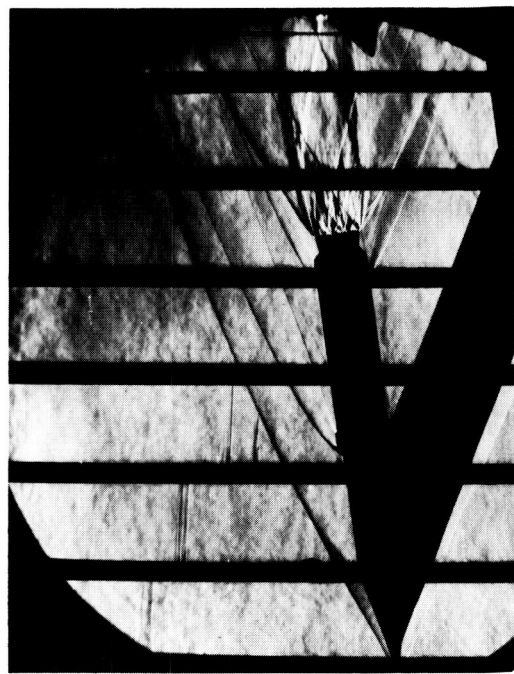
L-63-4706

Figure 19.- Typical schlieren photographs of configuration with shroud cut to fire wall. $\alpha = -8°$; $\delta_n = 6°$.
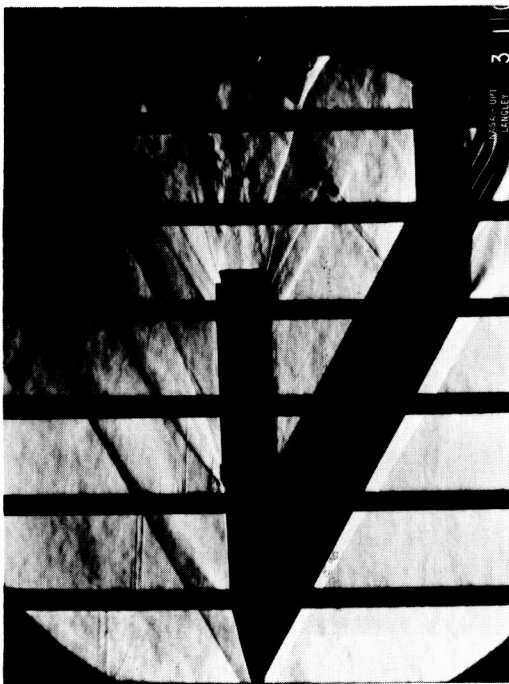
$\delta_n = 12°$; $\alpha = 0°$; $p_j/p_\infty = 11.4$; $M_\infty = 2.40$

$\delta_n = 6°$; $\alpha = -8°$; $p_j/p_\infty = 25.0$; $M_\infty = 2.87$

$\delta_n = 6°$; $\alpha = 0°$; $p_j/p_\infty = 0$; $M_\infty = 2.40$

$\delta_n = 12°$; $\alpha = -8°$; $p_j/p_\infty = 11.4$; $M_\infty = 2.40$

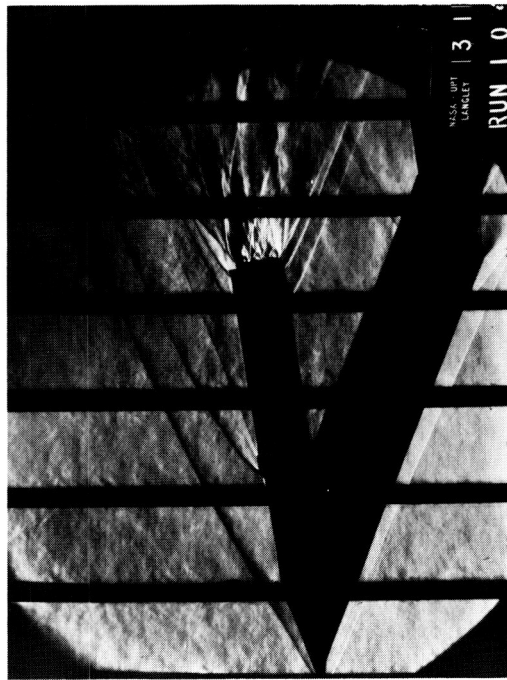Figure 20.- Typical schlieren photographs of configuration with shroud cut to heat shield.   L-63-4707

α=0°; p_j/p_∞=23.5; M_∞=2.87

α=-8°; p_j/p_∞=23.5; M_∞=2.87

α=0°; p_j/p_∞=11.5; M_∞=2.40

α=-8°; p_j/p_∞=11.5; M_∞=2.40

Figure 21.- Typical schlieren photographs of double-flare shroud configuration. δ_n = -3°.
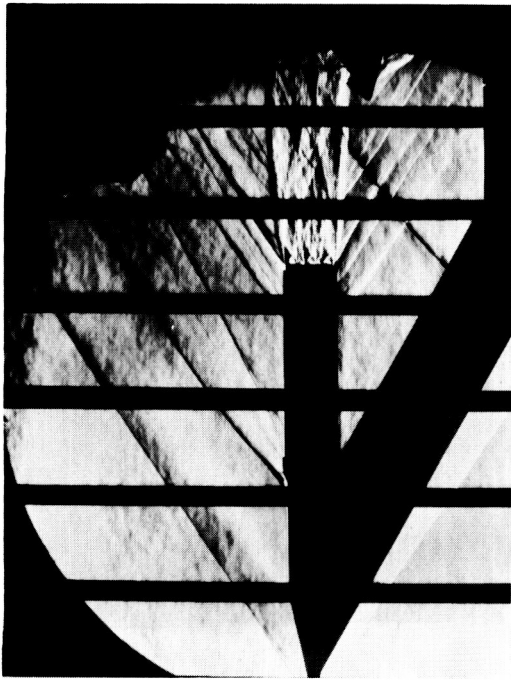
L.-63-4708

α=-8°; p_j/p_∞ =6.3; M_∞ =2.00

α=-8°; p_j/p_∞ =23.4°; M_∞ =2.87

α=0°; p_j/p_∞ =6.3; M_∞ =2.00

α=0°; p_j/p_∞ =23.5°; M_∞ =2.87

Figure 22.- Typical schlieren photographs of basic single-flare shroud configuration. $\delta_n = 6°$. L-63-4709